Published by Institute of Physics Publishing for SISSA

Received: *February 29, 2008*
Revised: *March 17, 2008*
Accepted: *March 27, 2008*
Published: *April 14, 2008*

Sparticles at the LHC

Daniel Feldman, Zuowei Liu and Pran Nath

Department of Physics, Northeastern University,
Boston, MA 02115, U.S.A.
E-mails: feldman.da@neu.edu, liu.zu@neu.edu, nath@neu.edu

Abstract: Sparticle mass hierarchies will play an important role in the type of signatures that will be visible at the Large Hadron Collider. We analyze these hierarchies for the four lightest sparticles for a general class of supergravity unified models including nonuniversalities in the soft breaking sector. It is shown that out of nearly 10^4 possibilities of sparticle mass hierarchies, only a small number survives the rigorous constraints of radiative electroweak symmetry breaking, relic density and other experimental constraints. The signature space of these mass patterns at the Large Hadron Collider is investigated using a large set of final states including multi-leptonic states, hadronically decaying τs, tagged b jets and other hadronic jets. In all, we analyze more than 40 such lepton plus jet and missing energy signatures along with several kinematical signatures such as missing transverse momentum, effective mass, and invariant mass distributions of final state observables. It is shown that a composite analysis can produce significant discrimination among sparticle mass patterns allowing for a possible identification of the source of soft breaking. While the analysis given is for supergravity models, the techniques based on mass pattern analysis are applicable to wide class of models including string and brane models.

Keywords: Supersymmetry Breaking, Supersymmetry Phenomenology, Supergravity Models, Beyond Standard Model.

JHEP04(2008)054

Contents

JHEP04(2008)054

1. Introduction

Supersymmtery (SUSY) remains a leading candidate to describe new physics beyond that of the Standard Model (SM). Recently, an approach for identifying supersymmetric particles (sparticles) was proposed involving sparticle mass hierarchies, or sparticle mass patterns. Such patterns could yield distinct identifiable signatures at the Fermilab's Tevatron and at the CERN Large Hadron Collider (LHC) [1, 2]. At the same time, the hierarchical mass patterns are model dependent and the determinations of such patterns could be helpful in extrapolating the data back to the theoretical model. This new approach has been

investigated within the framework of gravity mediated breaking of supersymmetry [3 – 5] and specifically within the minimal supergravity grand unified model, the mSUGRA model [3] (for a review see [6]) with sparticle mass ranges that lie within reach of the present colliders (for a review of recent search strategies see [7]). The analysis of [1, 2] was a rather brief introduction to the technique. Here we carry out a more in depth analysis within models with both universal and nonuniversal soft supersymmetry breaking [8 – 10]. Thus, in the minimal supersymmetric extension of the Standard Model (MSSM) there are 32 supersymmetric particles. We list them here to set notation. There are 4 Higgs boson states, of which three (h, H, A) are neutral, the first two being CP even and the third CP odd, and one charged Higgs $H^{\pm}$. In the gaugino-Higgsino sector there are two charged mass eigenstates (charginos) $\tilde{\chi}^{\pm}_{i=1,2}$, four charge neutral states (neutralinos) $\tilde{\chi}^{0}_{i=1,4}$, and the gluino $\tilde{g}$. In the sfermion sector, before diagonalization, there are 9 scalar leptons (sleptons) which are superpartners of the leptons with left and right chirality and are denoted as: $\{\tilde{e}_{L,R}, \tilde{\mu}_{L,R}, \tilde{\tau}_{L,R}, \tilde{\nu}_{e_L}, \tilde{\nu}_{\mu_L}, \tilde{\nu}_{\tau_L}\}$. Finally there are 12 squarks which are the superpartners of the quarks and are represented by: $\{\tilde{u}_{L,R}, \tilde{c}_{L,R}, \tilde{t}_{L,R}, \tilde{d}_{L,R}, \tilde{s}_{L,R}, \tilde{b}_{L,R}\}$. Mass diagonal slepton and squark states will in general be mixtures of L, R states.

If the 32 masses are treated as essentially all independent, aside from sum rules (for a pedagogical analysis on sum rules in the context of unification and RG analysis see [12]) on the Higgs, sfermions, chargino and neutralino masses, then without imposition of any phenomenological constraints, the number of hierarchical patterns for the sparticles could be as many as $O(10^{28})$ or larger. This represents a mini landscape in a loose way reminiscent of the string landscape (which, however, is much larger with as many as $O(10^{1000})$ possibilities). [Here we refer to the landscape of mass hierarchies and not to the landscape of vacua as is the case when one talks of a string landscape. For the string case the landscape consists of a countably discrete set, while for the case considered here, since the parameters can vary continuously, the landscape of vacua is indeed much larger. However, our focus will be the landscape of mass hierarchies.] Now, the number of possibilities can be reduced by very significant amounts in supergravity models with the imposition of the constraints of radiative electroweak symmetry breaking (REWSB),[1] and other phenomenological constraints. This was precisely what was accomplished in the analysis of [1, 2]. The analysis of ref. [1, 2] focused on the mass hierarchies for the first four lightest sparticles, and found the residual number of hierarchies to be 22 in mSUGRA. Here, the possible signatures from some of the patterns were also discussed along with the prospects for direct detection of dark matter within various mass hierarchies.

The phenomenology of supergravity (SUGRA) models has been discussed since their inception and there exists a considerable amount of literature regarding the implications of SUGRA (for early works see [11, 13], for more recent works see [14 – 16], for works with nonuniversalities see [17], and for works with hierarchical breaking and with U(1) gauge extensions see [18 – 20]). While many analyses of the mSUGRA parameter space have been

[1] EWSB can be realized non-radiatively for certain choices of parameters in the presence of nonuniversalities in the Higgs sector. Since in this analysis boundary conditions have been imposed at the GUT scale and RGEs have been used to obtain the low energy physics, we will retain this terminology in the subsequent descriptions of EWSB.

JHEP04(2008)054

limited to the case of vanishing trilinear couplings, several recent works [21 – 24, 15, 16, 25, 26] have appeared relaxing this assumption, and new portions of the parameter space have been found consistent with all known experimental constraints on the model.

In this paper we give a more exhaustive analysis of sparticle mass hierarchies for SUGRA models including nonuniversalities and also carry out a more detailed analysis of the signatures arising from these patterns. We further focus on ways in which patterns can be discriminated from each other using the relevant distinctive features of the signature space. It is found that for some model points one encounters the phenomenon where two distinct points in the parameter space of soft breaking may yield the same signatures within a 2σ error bar. We also discuss in this paper how such signature degeneracies can sometimes be lifted by an increased integrated luminosity. Finally, we discuss the issue of how well the soft parameters m_0 and $m_{1/2}$ (where m_0, $m_{1/2}$ are the mass parameters in mSUGRA models defined in section 2) may eventually be determined at the LHC which allows one to obtain an estimate on the resolution of these parameters using optimal LHC luminosities.

The outline of the rest of the paper is as follows: In section 2 we give a discussion of the sparticle landscape. Specifically, the landscape for the 4 lightest sparticles (in addition to the lightest Higgs boson) for the mSUGRA case is discussed in section 2.1 and the landscape for the 4 lightest sparticles for the nonuniversal SUGRA case is discussed in section 2.2. This includes cases with nonuniversalities in the Higgs sector, nonuniversalities in the third generation sector, and nonuniversalities in the gaugino sector. In section 2.3, we also discuss the possible number of mass patterns that can arise for the above case, as well as for the case when all 32 sparticle masses are taken into account. An analysis of the patterns and their origin in the space of soft breaking parameters is given in section 3. An analysis of the benchmarks for the landscape of 4 sparticle patterns is given in section 3.2. Section 4 is devoted to the discussion of the sparticle signatures at the LHC. In section 4.1 we give a discussion of the various SUSY tools that are utilized in this analysis. We discuss technical details of the analysis of the LHC signatures we have investigated in section 4.2. We then move on to discuss how one can distinguish sparticle mass patterns arising in mSUGRA in section 4.3, and sparticle mass patterns in SUGRA with nonuniversalities in section 4.4. The trileptonic signal as a tool to distinguish patterns is discussed in section 4.5. We utilize both event counting signatures and kinematical signatures in our analysis, the latter being discussed in section 4.6. In section 4.7, a method for distinguishing patterns utilizing a large set of signatures is also given. We discuss the signature space degeneracy among different models and how to lift it in section 5.1, and then we generalize our analysis to investigate the resolving power of the LHC with regards to its ability to probe the soft parameter space in section 5.2. Conclusions are given in section 6. Some of our longer tables have been relegated to the appendix.

2. The sparticle landscape

The analysis proceeds by specifying the model input parameters at the GUT scale, $M_G \sim 2 \times 10^{16}$ GeV, (no flavor mixing is allowed at the GUT scale) and using the renormal-

JHEP04(2008)054

ization group equations (RGEs) to predict the sparticle masses and mixing angles at the electroweak scale. The RGE code used to obtain the mass spectrum is SuSpect 2.34 [27], which is the default RGE calculator in MicrOMEGAs version 2.0.7 [28]. We have also investigated other RGE programs including ISASUGRA/ISAJET [29], SPheno [30] and SOFTSUSY [31]. We have cross checked our analysis using different codes and find no significant disagreement in most regions of the parameter space. The largest sensitivity appears to arise for the case of large $\tan\beta$ and the analysis is also quite sensitive to the running bottom mass and to the top pole mass (we take $m_b^{\overline{\rm MS}}(m_b) = 4.23$ GeV and $m_t(\text{pole}) = 170.9$ GeV in this analysis). Such sensitivities and their implications for the analysis of relic density calculations are well known in the literature [32] and a detailed comparison for various codes can be found in refs. ([33 – 36]).

Below we give the relevant constraints from collider and astrophysical data that are applied throughout the analysis unless stated otherwise.

1. WMAP 3 year data: The lightest R-Parity odd supersymmetric particle (LSP) is assumed charge neutral. The constraint on the relic abundance of dark matter under the assumption the relic abundance of neutralinos is the dominant component places the bound: $0.0855 < \Omega_{\widetilde{\chi}_1^0} h^2 < 0.1189 \;\; (2\sigma)$ [37].

2. As is well known sparticle loop exchanges make a contribution to the FCNC process $b \to s\gamma$ which is of the same order as the Standard Model contributions (for an update of SUSY contributions see [38]). The experimental limits on $b \to s\gamma$ impose severe constraints on the SUSY parameter space and we use here the constraints from the Heavy Flavor Averaging Group (HFAG) [39] along with the BABAR, Belle and CLEO experimental results: $\mathcal{B}r(b \to s\gamma) = (355 \pm 24^{+9}_{-10} \pm 3) \times 10^{-6}$. A new estimate of $\mathcal{B}r(\bar{B} \to X_s\gamma)$ at $O(\alpha_s^2)$ gives [40] $\mathcal{B}r(b \to s\gamma) = (3.15 \pm 0.23) \times 10^{-4}$ which moves the previous SM mean value of 3.6×10^{-4} a bit lower. In order to accommodate this recent analysis on the SM mean, as well as the previous analysis, we have taken a wider 3.5σ error corridor around the HFAG value in our numerical analysis. The total $\mathcal{B}r(\bar{B} \to X_s\gamma)$ including the sum of SM and SUSY contributions are constrained by this corridor. With a 2σ corridor, while some of the allowed points in our analysis will be eliminated, the main results of our pattern analysis remain unchanged.

3. The process $B_s \to \mu^+\mu^-$ can become significant for large $\tan\beta$ since the decay has a leading $\tan^6\beta$ [41] dependence and thus large $\tan\beta$ could be constrained by the experimental limit $\mathcal{B}r(B_s \to \mu^+\mu^-) < 1.5 \times 10^{-7}$ (90% CL), 2.0×10^{-7} (95% CL) [42]. This limit has just recently been updated [43] and gives $\mathcal{B}r(B_s \to \mu^+\mu^-) < 1.2 \times 10^{-7}$ (95% CL). Preliminary analyses [44] have reported the possibility of even more stringent constraints by a factor of 10. We take a more conservative approach in this analysis and allow model points subject to the bound $\mathcal{B}r(B_s \to \mu^+\mu^-) < 9 \times 10^{-6}$ (for a review see [45]).

4. Additionally, we also impose a lower limit on the lightest CP even Higgs boson mass. For the Standard Model like Higgs boson this limit is ≈ 114.4 GeV [46], while a limit of

JHEP04(2008)054

108.2 GeV at 95% CL is set on the production of an invisibly decaying Standard Model like Higgs by OPAL [47]. For the MSSM we take the constraint to be $m_h > 100$ GeV. A relaxation of the light Higgs mass constraint by 8 - 10 GeV affects mainly the analysis of SUGRA models where the stop mass can be light. However, light stops are possible even with the strictest imposition of the LEP bounds on the SM Higgs Boson. We take the other sparticle mass constraints to be $m_{\widetilde{\chi}_1^\pm} > 104.5$ GeV [48] for the lighter chargino, $m_{\widetilde{t}_1} > 101.5$ GeV for the lighter stop, and $m_{\widetilde{\tau}_1} > 98.8$ GeV for the lighter stau.

In addition to the above one may also consider the constraints from the anomalous magnetic moment of the muon. It is known that the supersymmetric electroweak corrections to $g_\mu - 2$ can be as large or larger than the Standard Model electroweak corrections [49]. The implications of recent experimental data has been discussed in several works (see, e.g. [50]). As in [23], here we use a rather conservative bound $-11.4 \times 10^{-10} < g_\mu - 2 < 9.4 \times 10^{-9}$.

2.1 The mSUGRA landscape for the 4 lightest sparticles

One mSUGRA model is a point in a 4 dimensional parameter space spanned by m_0, $m_{1/2}$, A_0, $\tan\beta$, and the sign of μ, where m_0 is the universal scalar mass, $m_{1/2}$ is the universal gaugino mass, A_0 is the universal trilinear coupling, $\tan\beta$ is the ratio of the two Higgs VEVs in the MSSM, and μ is the Higgs mixing parameter that enters via the term $\mu H_1 H_2$ in the superpotential. Typically scans of the parameter space are done by taking a vanishing trilinear coupling, and/or by looking at fixed values of $\tan\beta$ while varying (m_0, $m_{1/2}$). In this work we carry out a random scan in the 4-D input parameter space for fixed signs of μ with Monte Carlo simulations using flat priors under the following ranges of the input parameters

$$0 < m_0 < 4 \text{ TeV}, \quad 0 < m_{1/2} < 2 \text{ TeV} \quad |A_0/m_0| < 10, \quad 1 < \tan\beta < 60. \tag{2.1}$$

Since SUGRA models with $\mu > 0$ are favored by the experimental constraints much of the analysis presented here focuses on this case. Specifically for the $\mu > 0$ mSUGRA case, we perform a scan of the parameter space with a total of 2×10^6 trial parameter points. We delineate the patterns that emerge for the first four lightest sparticles. Here we find that at least sixteen hierarchical mass patterns emerge which are labeled as mSPs (minimal SUGRA Pattern). These mSPs can be generally classified according to the type of particle which is next heavier than the LSP, and we find four classes of patterns in mSUGRA: the chargino patterns (CP), the stau patterns (SUP), the stop patterns (SOP), and the Higgs patterns (HP), as exhibited below

1. Chargino patterns (CP) : mSP1, mSP2, mSP3, mSP4
2. Stau patterns (SUP) : mSP5, mSP6, mSP7, mSP8, mSP9, mSP10
3. Stop patterns (SOP) : mSP11, mSP12, mSP13
4. Higgs patterns (HP) : mSP14, mSP15, mSP16.

JHEP04(2008)054

mSP	Mass Pattern	$\mu > 0$	$\mu < 0$
mSP1	$\widetilde{\chi}_1^0 < \widetilde{\chi}_1^\pm < \widetilde{\chi}_2^0 < \widetilde{\chi}_3^0$	Y	Y
mSP2	$\widetilde{\chi}_1^0 < \widetilde{\chi}_1^\pm < \widetilde{\chi}_2^0 < A/H$	Y	Y
mSP3	$\widetilde{\chi}_1^0 < \widetilde{\chi}_1^\pm < \widetilde{\chi}_2^0 < \widetilde{\tau}_1$	Y	Y
mSP4	$\widetilde{\chi}_1^0 < \widetilde{\chi}_1^\pm < \widetilde{\chi}_2^0 < \widetilde{g}$	Y	Y
mSP5	$\widetilde{\chi}_1^0 < \widetilde{\tau}_1 < \widetilde{l}_R < \widetilde{\nu}_\tau$	Y	Y
mSP6	$\widetilde{\chi}_1^0 < \widetilde{\tau}_1 < \widetilde{\chi}_1^\pm < \widetilde{\chi}_2^0$	Y	Y
mSP7	$\widetilde{\chi}_1^0 < \widetilde{\tau}_1 < \widetilde{l}_R < \widetilde{\chi}_1^\pm$	Y	Y
mSP8	$\widetilde{\chi}_1^0 < \widetilde{\tau}_1 < A \sim H$	Y	Y
mSP9	$\widetilde{\chi}_1^0 < \widetilde{\tau}_1 < \widetilde{l}_R < A/H$	Y	Y
mSP10	$\widetilde{\chi}_1^0 < \widetilde{\tau}_1 < \widetilde{t}_1 < \widetilde{l}_R$	Y	
mSP11	$\widetilde{\chi}_1^0 < \widetilde{t}_1 < \widetilde{\chi}_1^\pm < \widetilde{\chi}_2^0$	Y	Y
mSP12	$\widetilde{\chi}_1^0 < \widetilde{t}_1 < \widetilde{\tau}_1 < \widetilde{\chi}_1^\pm$	Y	Y
mSP13	$\widetilde{\chi}_1^0 < \widetilde{t}_1 < \widetilde{\tau}_1 < \widetilde{l}_R$	Y	Y
mSP14	$\widetilde{\chi}_1^0 < A \sim H < H^\pm$	Y	
mSP15	$\widetilde{\chi}_1^0 < A \sim H < \widetilde{\chi}_1^\pm$	Y	
mSP16	$\widetilde{\chi}_1^0 < A \sim H < \widetilde{\tau}_1$	Y	
mSP17	$\widetilde{\chi}_1^0 < \widetilde{\tau}_1 < \widetilde{\chi}_2^0 < \widetilde{\chi}_1^\pm$		Y
mSP18	$\widetilde{\chi}_1^0 < \widetilde{\tau}_1 < \widetilde{l}_R < \widetilde{t}_1$		Y
mSP19	$\widetilde{\chi}_1^0 < \widetilde{\tau}_1 < \widetilde{t}_1 < \widetilde{\chi}_1^\pm$		Y
mSP20	$\widetilde{\chi}_1^0 < \widetilde{t}_1 < \widetilde{\chi}_2^0 < \widetilde{\chi}_1^\pm$		Y
mSP21	$\widetilde{\chi}_1^0 < \widetilde{t}_1 < \widetilde{\tau}_1 < \widetilde{\chi}_2^0$		Y
mSP22	$\widetilde{\chi}_1^0 < \widetilde{\chi}_2^0 < \widetilde{\chi}_1^\pm < \widetilde{g}$		Y

Table 1: Hierarchical mass patterns for the four lightest sparticles in mSUGRA when $\mu < 0$ and $\mu > 0$. The patterns can be classified according to the next to the lightest sparticle. For the mSUGRA analysis the next to the lightest sparticle is found to be either a chargino, a stau, a stop, a CP even/odd Higgs, or the next lightest neutralino $\widetilde{\chi}_2^0$. The notation A/H stands for either A or H. In mSP14-mSP16 it is possible that the Higgses become lighter than the LSP. Y stands for appearance of the pattern for the sub case.

The hierarchical mass patterns mSP1-mSP16 are defined in table 1. We note that the pattern mSP7 appears in the analyses of [51 – 53].

We also performed a similar scan for the mSUGRA with $\mu < 0$ case using the Monte Carlo simulation with flat priors and the same parameter ranges as specified in eq. (2.1). Most of the mSP patterns that appear in the $\mu > 0$ case also appear in the $\mu < 0$ case (see table 1). However, in addition one finds new patterns shown below

1. Stau patterns (SUP) : mSP17, mSP18, mSP19

2. Stop patterns (SOP) : mSP20, mSP21

3. Neutralino patterns (NP) : mSP22.

JHEP04(2008)054

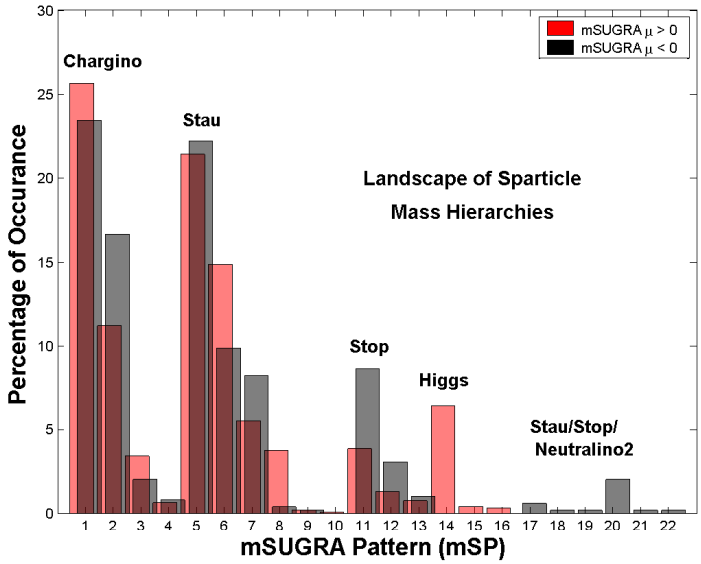

Figure 1: Distribution of the surviving hierarchical mass patterns in the landscape for the mSUGRA model with $\mu > 0$ (light) and $\mu < 0$ (dark), under various constraints as discussed in the text.

Snowmass	mSP
SPS1a, SPS1b, SPS5	mSP7
SPS2	mSP1
SPS3	mSP5
SPS4, SPS6	mSP3

Post-WMAP3	mSP
$A', B', C', D', G', H', J', M'$	mSP5
I', L'	mSP7
E'	mSP1
K'	mSP6

CMS LM/HM	mSP
LM1, LM6, HM1	mSP5
LM2, LM5, HM2	mSP7
LM3, LM7, LM8, LM9, LM10, HM4	mSP1
LM4, HM3	mSP3

Table 2: Mapping between the mSPs and the Snowmass, Post-WMAP3, and CMS benchmark points. The points $B' =$ LM1, $I' =$ LM2, $C' =$ LM6. HM1 in SuSpect has $m_{\widetilde{\chi}_1^0} > m_{\widetilde{\tau}_1}$, but this is not the case for ISAJET, SPheno, and SOFTSUSY. Among the CMS benchmarks, only LM1, LM2, LM6, and HM1, HM2 are capable of giving the correct relic density. Thus the mapping above applies only to the mass pattern, while all of our mSP and NUSP benchmark points satisfy the relic density constraints from MicrOMEGAs with SuSpect. The CMS test points do a better job of representing mSP1 which is the dominant pattern found in our analysis. There are no HP test points or SOP test points in any of the previous works.

JHEP04(2008)054

We note that the analysis of ref. [54] has a sparticle spectrum which corresponds to mSP11 and contains light stops. Light stops have also been discussed recently in [55, 25].

While the earlier works which advocated benchmark points and slopes made good progress in systematizing the search for supersymmetry, we find that they do not cover the more broad set of possible mass hierarchies we discuss here. That is, many of the mSP patterns do not appear in the earlier works that advocated benchmark points for SUSY searches. For example the Snowmass mSUGRA points (labeled SPS) [56] and the Post-WMAP benchmark points of [57], make up only a small fraction of the possible mass hierarchies listed in table 1. The CMS benchmarks classified as Low Mass (LM) and High Mass (HM) [58] (for a recent review see [59, 60]) does a good job covering the mSP1 pattern which appears as the most dominant pattern in our analysis, but there are no Higgs patterns or stop patterns discussed in the CMS benchmarks as well as in SPS or in Post-WMAP benchmarks. We exhibit the mapping of mSPs with other benchmarks points in a tabular form in table 2.

In figure 1 we give the relative distribution of these hierarchies found in our Monte Carlo scan. The most common patterns found are CPs and SUPs, especially mSP1 and mSP5. However there exists a significant region of the parameter space where SOPs and HPs can be realized. The percentages of occurrence of the various patterns in the mSUGRA landscape for both μ positive and μ negative are exhibited in figure 1. The analysis of figure 1 shows that the chargino patterns (CP) are the most dominant patterns, followed by the stau patterns (SUP), the stop patterns (SOP), and the Higgs patterns (HP). In contrast, most emphasis in the literature, specifically in the context of relic density analysis, has focused on the stau patterns, with much less attention on other patterns. Specifically the Higgs patterns have hardly been investigated or discussed. The exceptions to this, in the context of the Higgs patterns, are the more recent works of refs. [1, 2], and similar mass ranges for the Higgs bosons have been studied in [61] (see also [62]).

2.2 The landscape of the 4 lightest sparticles in NUSUGRA

Next we discuss the landscape of the 4 lightest sparticles for the case of nonuniversal supergravity models. Here we consider nonuniversalities in the Higgs sector (NUH), in the third generation sector (NU3), and in the gaugino sector (NUG). Such nonuniversalities appear quite naturally in supergravity models with a non-minimal Kähler potential, and in string and D-Brane models. The parametrization of the nonuniversalities is given by

$$\begin{aligned} &\text{NUH}: M_{H_u} = m_0(1+\delta_{H_u}), \quad M_{H_d} = m_0(1+\delta_{H_d}), \\ &\text{NU3}: M_{q3} = m_0(1+\delta_{q3}), \quad M_{u3,d3} = m_0(1+\delta_{tbR}), \\ &\text{NUG}: M_1 = m_{1/2}, \qquad\qquad M_{2,3} = m_{1/2}(1+\delta_{M_{2,3}}). \end{aligned} \tag{2.2}$$

In the above δ_{H_u} and δ_{H_d} define the nonuniversalities for the up and down Higgs mass parameters, M_{q3} is the left-handed squark mass for the 3rd generation, and M_{u3} (M_{d3}) are the right-handed u-squark (d-squark) masses for the 3rd generation. The nonuniversalities in the gaugino sector are parameterized here by δ_{M_2} and δ_{M_3}. We have carried out a Monte Carlo scan with flat priors using 10^6 model points in each of the three types of NUSUGRA models, taking the same input parameter ranges as specified in eq. (2.1) and $-0.9 \leqslant \delta \leqslant 1$.

JHEP04(2008)054

NUSP	Mass Pattern	NU3	NUG
NUSP1	$\widetilde{\chi}_1^0 < \widetilde{\chi}_1^\pm < \widetilde{\chi}_2^0 < \widetilde{t}_1$	Y	Y
NUSP2	$\widetilde{\chi}_1^0 < \widetilde{\chi}_1^\pm < A \sim H$	Y	
NUSP3	$\widetilde{\chi}_1^0 < \widetilde{\chi}_1^\pm < \widetilde{\tau}_1 < \widetilde{\chi}_2^0$		Y
NUSP4	$\widetilde{\chi}_1^0 < \widetilde{\chi}_1^\pm < \widetilde{\tau}_1 < \widetilde{l}_R$		Y
NUSP5	$\widetilde{\chi}_1^0 < \widetilde{\tau}_1 < \widetilde{\nu}_\tau < \widetilde{\tau}_2$	Y	
NUSP6	$\widetilde{\chi}_1^0 < \widetilde{\tau}_1 < \widetilde{\nu}_\tau < \widetilde{\chi}_1^\pm$	Y	
NUSP7	$\widetilde{\chi}_1^0 < \widetilde{\tau}_1 < \widetilde{t}_1 < A/H$		Y
NUSP8	$\widetilde{\chi}_1^0 < \widetilde{\tau}_1 < \widetilde{l}_R < \widetilde{\nu}_\mu$		Y
NUSP9	$\widetilde{\chi}_1^0 < \widetilde{\tau}_1 < \widetilde{\chi}_1^\pm < \widetilde{l}_R$		Y
NUSP10	$\widetilde{\chi}_1^0 < \widetilde{t}_1 < \widetilde{g} < \widetilde{\chi}_1^\pm$		Y
NUSP11	$\widetilde{\chi}_1^0 < \widetilde{t}_1 < A \sim H$		Y
NUSP12	$\widetilde{\chi}_1^0 < A \sim H < \widetilde{g}$		Y
NUSP13	$\widetilde{\chi}_1^0 < \widetilde{g} < \widetilde{\chi}_1^\pm < \widetilde{\chi}_2^0$		Y
NUSP14	$\widetilde{\chi}_1^0 < \widetilde{g} < \widetilde{t}_1 < \widetilde{\chi}_1^\pm$		Y
NUSP15	$\widetilde{\chi}_1^0 < \widetilde{g} < A \sim H$		Y

Table 3: New 4 sparticle mass patterns that arise in NUSUGRA over and above the mSP patterns of table 1. These are labeled nonuniversal SUGRA patterns (NUSP) and at least 15 new patterns are seen to emerge which are denoted by NUSP1-NUSP15.

Almost all of the mSP patterns seen for the mSUGRA cases were found in supergravity models with nonuniversal soft breaking, as the mSUGRA model is contained within the nonuniversal supergravity models. In addition we find many new patterns labeled NUSPs (nonuniversal SUGRA pattern), and they are exhibited in table 3.

As in the mSUGRA case one finds several pattern classes, CPs, SUPS, SOPs, and HPs as exhibited below. In addition, we find several Gluino patterns (GP) where the gluino is the NLSP.

1. Chargino patterns (CP) : NUSP1, NUSP2, NUSP3, NUSP4
2. Stau patterns (SUP) : NUSP5, NUSP6, NUSP7, NUSP8, NUSP9
3. Stop patterns (SOP) : NUSP10, NUSP11
4. Higgs patterns (HP) : NUSP12
5. Gluino patterns (GP) : NUSP13, NUSP14, NUSP15.

It is interesting to note that for the 4 sparticle landscape we find saturation in the number of mass hierarchies that are present. For example, for the case $\mu > 0$ in mSUGRA , increasing the soft parameter scan from 1×10^6 parameter model points to 2×10^6 model points does not increase the number of 4 sparticle patterns. In this context it becomes relevant to examine as to what degree the relic density and other experimental constraints play a role in constraining the parameter space and thus reducing the number of patterns.

JHEP04(2008)054

Model Type	Trial Models	Output Models	No. of Patterns	Relic Density Constraints	No. of Patterns	All Constraints	No. of Patterns
mSUGRA($\mu > 0$)	10^6	265,875	55	1,360	22	902	16
mSUGRA($\mu < 0$)	10^6	226,991	63	1,000	31	487	18
NUH($\mu > 0$)	10^6	222,023	59	1,024	24	724	15
NU3($\mu > 0$)	10^6	229,928	73	970	28	650	20
NUG($\mu > 0$)	10^6	273,846	103	1,788	36	1,294	28

Table 4: An analysis of mass patterns for the four lightest sparticles. Exhibited in the table are the model type, the number of trial input points for each model, the number surviving the radiative electroweak symmetry breaking scheme as given by SuSpect (column 3), the number surviving when the relic density constraints are applied with MicrOMEGAs (column 5), the number surviving with inclusion of all experimental collider constraints (column 7), along with the corresponding number of hierarchical mass patterns in each case (column 8).

This is exhibited in table 4 where we demonstrate how the relic density and the other experimental constraints decrease the number of admissible model points in the allowed parameter space for the mSUGRA models with both $\mu > 0$ and $\mu < 0$, and also for the cases with nonuniversalities in the Higgs sector, nonuniversalities in the third generation sector, and with nonuniversalities in the gaugino sector. In each case we start with 10^6 model points at the GUT scale, and find that the electroweak symmetry breaking constraints reduce the number of viable models to about 1/4 of what we started with. We find that the allowed number of models translates into SUGRA mass patterns which are typically less than 100. The admissible set of parameter points reduces drastically when the relic density constraints are imposed and are then found to typically reduce the number of models by a factor of about 200 or more, with a reduction in the number of allowed patterns by a factor of 2 or more. Inclusion of all other experimental constraints further reduces the number of admissible points by a factor between 30% and 50%, with a corresponding reduction in the number of patterns by up to 40%. The above analysis shows that there is an enormous reduction in the number of admissible models and the corresponding number of hierarchical mass patterns after the constraints of radiative breaking of the electroweak symmetry, relic density constraints, and other experimental constraints are imposed.

2.3 Hierarchical patterns for the full sparticle spectrum

We discuss now the number of hierarchical mass patterns for the full set of 32 sparticles in SUGRA models when the constraints of electroweak symmetry, relic density, and other experimental constraints are imposed. The result of the analysis is given in figure 2 and table 5.

Here one finds that increasing the number of model points in the scan does increase the number of patterns. However, the ratio of the number of patterns to the total number of models that survive all the constraints from the scan decreases sharply as shown in the right panel of figure 2. This means that although saturation is not yet achieved one is moving fast towards achieving saturation with a relatively small number of allowed patterns for all the 32 sparticles within SUGRA models consistent with the various experimental constraints. The analysis of table 5 shows that the number of allowed patterns for the 32

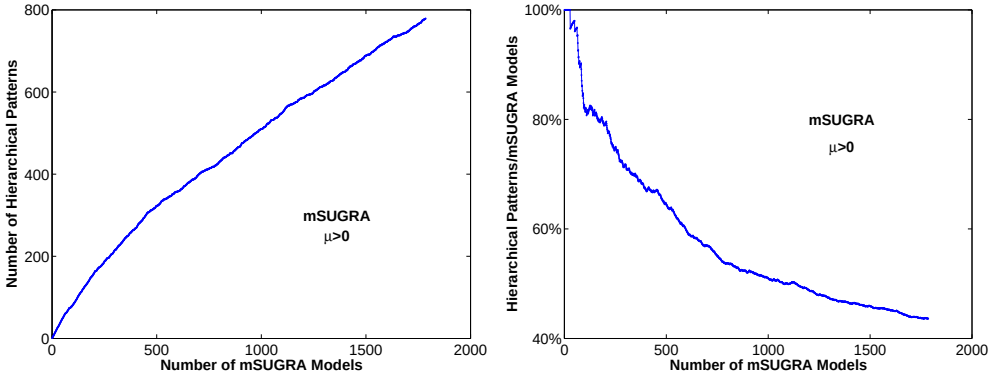

Figure 2: Left panel: The number of hierarchical mass patterns for 32 sparticles vs the number of trial points for mSUGRA models which survive the electroweak symmetry breaking constraints, the relic density and all other experimental constraints. The number of hierarchical mass patterns show a trend towards saturation. Right panel: A similar phenomenon is seen in the ratio between the number of patterns over the number of surviving trial points in mSUGRA models.

Models [No.]	No. after constraints	No. of patterns
mSUGRA($\mu > 0$) [10^6]	902	505
mSUGRA($\mu < 0$) [10^6]	487	268
NUH($\mu > 0$) [10^6]	724	517
NU3($\mu > 0$) [10^6]	650	528
NUG($\mu > 0$) [10^6]	1294	1092
All Above[5×10^6]	4057	2557

Table 5: The table exhibits a dramatic reduction of the landscape from upward of $\sim O(10^{28})$ hierarchical mass patterns for the 32 sparticle masses to a much smaller number when the electroweak symmetry breaking constraints, the relic density constraints, and other experimental constraints are applied. Column 1 shows one million input parameter points for each of the models investigated, and the number surviving all the constraints are exhibited in column 2, while column 3 gives the number of hierarchical patterns.

sparticles, which in the MSSM without the SUGRA framework can be as large as $O(10^{28})$ or larger, reduces rather drastically when various constraints are applied in supergravity models. We note that some patterns are repeated as we move across different model types listed in the first column of table 5. Thus the total number of patterns listed at the bottom of the last column of this table is smaller than the sum of patterns listed above in that column. We note that the precise number and nature of the patterns are dependent on the input parameters such as the top mass and a significant shift in the input values could modify the pattern structure.

3. Sparticle patterns and the nature of soft breaking

3.1 Correlating mass hierarchies with the soft parameter space

It is interesting to ask if the patterns can be traced back to some specific regions of the parameter of soft breaking from where they originate. This indeed is the case, at least, for

JHEP04(2008)054

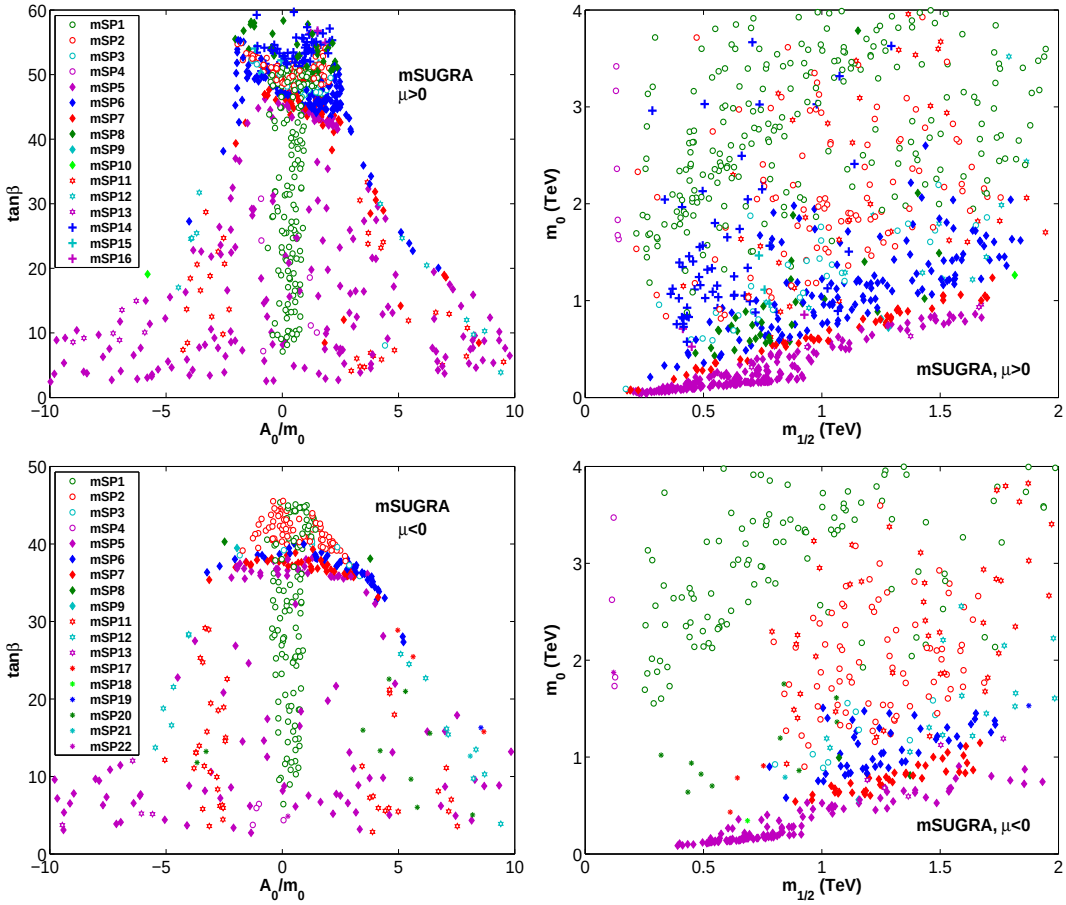

Figure 3: The dispersion of mSPs arising in mSUGRA in the $\tan\beta$ vs A_0/m_0 plane (left panels), and in the m_0 vs $m_{1/2}$ plane (right panels) for the $\mu > 0$ case (upper panels) and $\mu < 0$ case (lower panels). The analysis is based on a scan of 10^6 trial model points with flat priors in the ranges $m_0 < 4$ TeV, $m_{1/2} < 2$ TeV, $1 < \tan\beta < 60$, and $|A_0/m_0| < 10$. mSP1 is confined to the region where $|A_0/m_0| < 2$. For the case $\mu < 0$, no HPs are seen, and also, no model points survive in the region where $\tan\beta > 50$ in contrast to the $\mu > 0$ case where there is a significant number for $\tan\beta \gtrsim 45$.

some of the patterns. The analysis illustrating the origin of the patterns in the parameter space is given in figure 3. Exhibited are the landscape of sparticle mass spectra in the planes (I) $\tan\beta$ vs A_0/m_0 and (II) m_0 vs $m_{1/2}$, when the soft parameters are allowed to vary in the ranges given in eq. (2.1). Many interesting observations can be made from these spectral decompositions. For example, a significant set of the mSP1 (CP) models lie in the region $|A_0/m_0| < 2$ and correspond to the Hyperbolic branch(HB)/Focus Point (FP) [63] regions, while most of the SOPs have a rather large ratio of A_0/m_0 with the satisfaction of REWSB. In this analysis we require that there be no charge or color breaking (CCB) [64, 65] at the electroweak scale. We note in passing that it has been argued that even if the true minimum is not color or charge preserving, the early universe is likely to occupy the CCB

JHEP04(2008)054

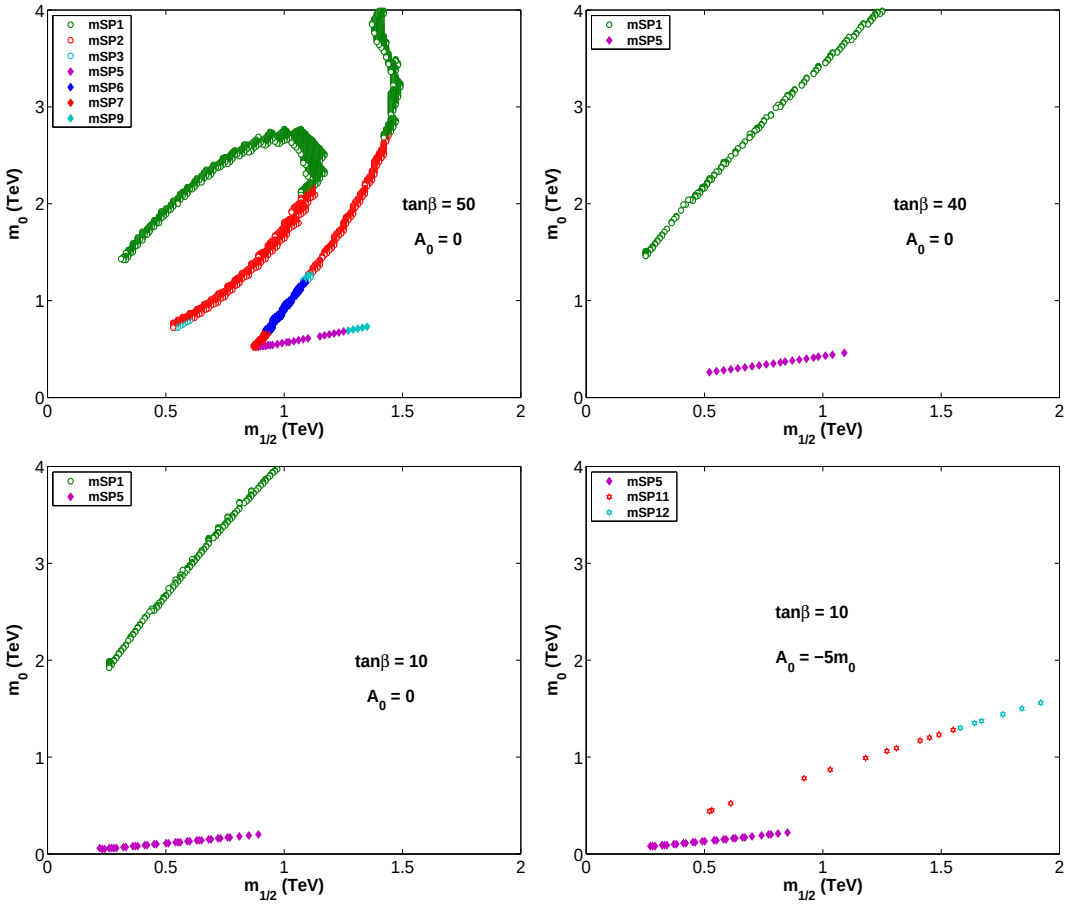

Figure 4: Dispersion of patterns in the m_0 vs $m_{1/2}$ plane for fixed values of $\tan\beta$ and A_0/m_0. The region scanned is in the range $m_0 < 4$ TeV and $m_{1/2} < 2$ TeV with a 10 GeV increment for each mass. Only a subset of the allowed parameter points relative to figure 3 remain, since the scans are on constrained surfaces in the mSUGRA parameter space.

preserving minimum and such minima may still be acceptable if the tunneling lifetime from the false to the true vacuum is much greater than the present age of the universe [66]. Next, we note that for the mSUGRA $\mu > 0$ case, the region around $\tan\beta = 50$ has a large number of models that can be realized, while the region around $\tan\beta = 30$ has far less model points. We also note that most of the HPs reside only in the very high $\tan\beta$ region in mSUGRA, but this situation can be changed significantly in the NUH case where HP points can be realized in the $\tan\beta$ region as low as $\tan\beta \sim 20$. In the m_0 vs $m_{1/2}$ plane, one finds that most of CPs and HPs have a larger universal scalar mass than most of the SUPs and SOPs.

Often in the literature one limits the analysis by fixing specific values of A_0 and $\tan\beta$. For A_0 the value most investigated is $A_0 = 0$. However, constraining the values of A_0 or of $\tan\beta$ artificially eliminates a very significant part of the allowed parameter space where all the relevant constraints (the REWSB constraint as well as the relic density and the

JHEP04(2008)054

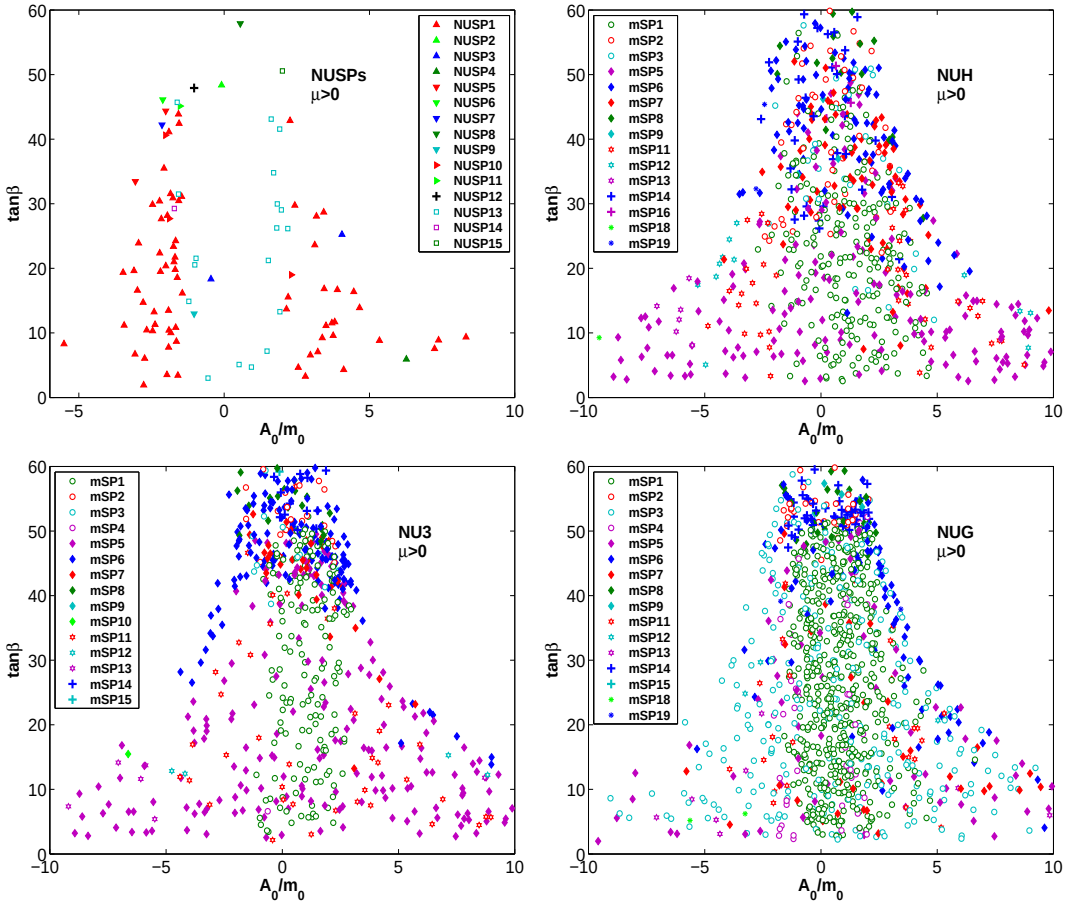

Figure 5: An exhibition of the NUSPs and mSPs for the NUH, NU3, and NUG models in the $\tan\beta$ vs A_0/m_0 plane. The range of SUGRA parameters are the same as the case mSUGRA ($\mu > 0$). One may notice that the mSP1 points arising from NU models lie in a relatively larger A_0/m_0 region. Most of the models in NU cases are still mSPs, and among the NUSPs, only two patterns have a relatively large population, these being NUSP1 and NUSP13. One may also notice that in NUH case, the HPs can exist in a low $\tan\beta$ region as opposed to the mSUGRA case where HPs can either exist in the large $\tan\beta$ region ($\mu > 0$) or are totally eliminated ($\mu < 0$).

experimental constraints) can be satisfied as seen in figure 3. One can extract the familiar plots one finds in the literature where A_0 and $\tan\beta$ are constrained from a reduction of the top-right panel of figure 3. The results of this reduction are shown in figure 4 with a focused scan in specific regions of the soft parameter space. Specifically the bottom-left and top-right panels of figure 4 show the familiar stau coannihilation [67, 68, 51] regions and the HB/FP branch, the bottom-right panel gives the stau coannihilation region and the stop coannihilation region because of the relatively large A_0 value, and the top-left panel is of the form seen in the works of Djouadi et al. [23] where the Higgs funnel plays an important role in the satisfaction of the relic density.

An analysis similar to that of figure 3 for the nonuniversal case is given in figure 5. Here

JHEP04(2008)054

in addition to the mSPs new patterns emerge which we label as nonuniversal sugra patterns or NUSPs. Among the NUSPs the dominant patterns are NUSP1 (CP) and NUSP13 (GP), which are seen to arise the model with nonuniversalities in the gaugino sector, i.e., the NUG model. In general, the NUG is dominated by the CP patterns whereas the NUH case is rather diverse offering the possibility of Higgs patterns at lower, less fine tuned values of $\tan\beta$.

3.2 Benchmarks for sparticle patterns

As discussed in section 2.1, many of the sparticle mass patterns discussed in this analysis do not appear in the Snowmass, Post-WMAP, and CMS benchmark points. With some of these mSP and NUSP having a significant probability of occurrence, we therefore provide a larger set of benchmark points for the various patterns in different SUGRA scenarios. These benchmark points are exhibited in tables 8, 9, 10, 11, 12 of the appendix. Each of these benchmarks satisfies the relic density and other experimental constraints with SuSpect linked to MicrOMEGAs. We have explicitly checked that the first mSP benchmark point in each of the tables can be reproduced by using SPheno, and SOFTSUSY by allowing minor variations on the input parameters. The benchmarks are chosen to cover wide parts of the SUGRA parameter space. We give these benchmarks, several for each mass pattern, as the search for SUSY from the point of view of mass patterns has important consequences for LHC experimental searches. Some of the patterns are correlated with certain well investigated phenomena such as the HB/FP branches of REWSB and the stau-neutralino co-annihilation regions. However, many of the patterns arise from multiple annihilation processes.

4. LHC signatures for mass patterns

4.1 Event generation and detector simulation

Before moving to the discussion of the LHC signatures arising from various mSPs and NUSPs, we first give a detailed description of our LHC simulation procedure.

After the imposition of all the constraints mentioned in the previous sections, such as the relic density constraints from WMAP data, the constraints on the FCNCs, as well as mass limits on the sparticle spectrum, we are left with the candidate model points for the signature analysis. For each of these model points, a SUSY Les Houches Accord (SLHA) file [70] is interfaced to PYTHIA 6.4.11 [71] through PGS4 [72] for the computation of SUSY production cross sections and branching fractions. In this analysis, for signals, we have generated all of PYTHIA's $2 \to 2$ SUSY production modes using MSEL = 39.[2] Leading order cross sections from PYTHIA and leading order cross sections from PROSPINO 2.0 [73] were cross checked against one another for consistency over several regions of the

[2]More specifically this choice generates 91 SUSY production modes including gaugino, squark, slepton, and SUSY Higgs pair production but leaves out singly produced Higgs production. For further details, see [71]. A treatment of singly produced Higgs production in the context of sparticle mass hierarchies was included in the analysis of ref. [2].

JHEP04(2008)054

soft parameter space. TAUOLA [74] is called by PGS4 for the calculation of tau branching fractions as controlled in the PYTHIA parameter card (.pyt) file. With PGS4 we use the Level 1 (L1) triggers based on the Compact Muon Solenoid detector (CMS) specifications [75, 58] and the LHC detector card. Muon isolation is controlled by employing the cleaning script in PGS4. We take the experimental nomenclature of lepton being defined only as electron or muon and thus distinguish electrons and muons from tau leptons. SM backgrounds have been generated with QCD multi-jet production due to light quark flavors, heavy flavor jets ($b\bar{b}$, $t\bar{t}$), Drell-Yan, single Z/W production in association with quarks and gluons ($Z+$ jets / $W+$ jets), and ZZ, WZ, WW pair production resulting in multi-leptonic backgrounds. Extraction of final state particles from the PGS4 event record is accomplished with a code SMART (= SUSY Matrix Routine) written by us [1] which provides an optimized processing of PGS4 event data files. The standard criteria for the discovery limit of new signals is that the SUSY signals should exceed either $5\sqrt{N_{\rm SM}}$ or 10 whichever is larger, i.e., $\mathrm{N_{SUSY}} > \mathrm{Max}\left\{5\sqrt{N_{\rm SM}}, 10\right\}$ and such a criteria is imposed where relevant. We have also cross checked various results of our analysis with three CMS notes [76 – 78] and we have found agreement with these works using SMART and PGS4 for signal and backgrounds.

We note that several works where sparticle signatures are discussed have appeared recently [79 – 84]. However, the issue of hierarchical mass patterns and the correlation of signatures with such patterns has not been discussed which is what the analysis of this work investigates.

4.2 Post trigger level cuts and LHC signatures

Generally speaking, there are two kinds of LHC signatures: (i) event counting signatures, and (ii) kinematical signatures. We have investigated both of these for the purpose of discriminating the sparticle mass patterns. We list our event counting signatures in table 6, where we have carried out analyses of a large set of lepton + jet signals. In our counting procedure, only electron and muon are counted as leptons, while tau jets are counted independently. For clarity, from here on, our use of 'jet(s)' will exclude tau jets. Thus, for jet identification, we divide jets into two categories: b-tagged jets and jets without b-tagging, which we simply label as b-jets and non-b-jets (see also [79]). There are some counting signatures that only concern one class of measurable events, for example, the number of events containing one tagged b-jet and any other final state particles. There are also types of signatures of final state particles with combinations of two or three different species. For instance, one such example would be the number of events in which there is a single lepton and a single tau.

When performing the analysis of event counting, for each SUGRA model point, we impose global post trigger cuts to analyze most of our PGS4 data. Below we give our default post trigger cuts which are used throughout the paper unless stated otherwise.

1. In an event, we only select photons, electrons, and muons that have transverse momentum $P_T^p > 10\,\mathrm{GeV}$ and $|\eta^p| < 2.4$, $p = (\gamma, e, \mu)$.

2. Taus which satisfy $P_T^\tau > 10\,\mathrm{GeV}$ and $|\eta^\tau| < 2.0$ are selected.

JHEP04(2008)054

Signature	Description	Signature	Description
0L	0 Lepton	0T	0 τ
1L	1 Lepton	1T	1 τ
2L	2 Leptons	2T	2 τ
3L	3 Leptons	3T	3 τ
4L	4 Leptons and more	4T	4 τ and more
0L1b	0 Lepton + 1 b-jet	0T1b	0 τ + 1 b-jet
1L1b	1 Lepton + 1 b-jet	1T1b	1 τ + 1 b-jet
2L1b	2 Leptons + 1 b-jet	2T1b	2 τ + 1 b-jet
0L2b	0 Lepton + 2 b-jets	0T2b	0 τ + 2 b-jets
1L2b	1 Lepton + 2 b-jets	1T2b	1 τ + 2 b-jets
2L2b	2 Leptons + 2 b-jets	2T2b	2 τ + 2 b-jets
ep	e^+ in 1L	em	e^- in 1L
mp	μ^+ in 1L	mm	μ^- in 1L
tp	τ^+ in 1T	tm	τ^- in 1T
OS	Opposite Sign Di-Leptons	0b	0 b-jet
SS	Same Sign Di-Leptons	1b	1 b-jet
OSSF	Opposite Sign Same Flavor Di-Leptons	2b	2 b-jets
SSSF	Same Sign Same Flavor Di-Leptons	3b	3 b-jets
OST	Opposite Sign Di-τ	4b	4 b-jets and more
SST	Same Sign Di-τ	TL	1 τ plus 1 Lepton

Kinematical signatures
1. $P_T^{\rm miss}$
2. Effective Mass = $P_T^{\rm miss} + \sum_j P_T^j$
3. Invariant Mass of all jets
4. Invariant Mass of e^+e^- pair
5. Invariant Mass of $\mu^+\mu^-$ pair
6. Invariant Mass of $\tau^+\tau^-$ pair

Table 6: The tables give a list of 40 counting signatures along with the kinematical signatures analyzed for each point in the SUGRA model parameter space. $L = e, \mu$ signifies only electrons and muons.

3. For hadronic jets, only those satisfying $P_T^j > 60\,\text{GeV}$ and $|\eta^j| < 3$ are selected.

4. We require a large amount of missing transverse momentum, $P_T^{\rm miss} > 200\,\text{GeV}$.

5. There are at least two jets that satisfy the P_T and η cuts.

Our default post trigger level cuts are standard and are designed to suppress the Standard Model background, and highlight the SUSY events over a broad class of models.

JHEP04(2008)054

The different kinematical signatures we investigated for the purpose of discriminating among sparticle mass patterns are also exhibited in table 6. One may further divide the kinematical signatures into two classes: namely those involving transverse momentum P_T and those which involve invariant mass. For those involving P_T, we have investigated missing P_T distributions and the effective mass, the latter being the sum of missing P_T and P_T of all jets contained within an event. For the kinematical variables using invariant mass, we reconstruct such quantities for four different cases, i.e., the invariant mass for all jets, for e^+e^- pair, for $\mu^+\mu^-$ pair, and for $\tau^+\tau^-$ pair. The reconstruction of the invariant mass of $\tau^+\tau^-$ pair is based on hadronically decaying taus (for recent analyses see [51]).

4.3 Discrimination among mSPs in mSUGRA

We turn now to a discussion of how one may distinguish among different patterns. The analysis begins by considering the 902 model points that survive our mSUGRA scan with 10^6 trial points, and simulating their LHC signals with PGS4 using, for illustration, $10\,\text{fb}^{-1}$ of integrated luminosity at the LHC. In our analysis we will focus mostly on the counting signatures. Here the most useful counting signature is the total number of SUSY events after trigger level cuts and post trigger level cuts are imposed. All other counting signatures are normalized with respect to the total number of SUSY events passing the cuts and thus appear as fractions lying between (0,1) in our figures. To keep the analysis statistically significant, we admit only those points in the parameter space that generate at least 500 total SUSY events.

We give now the details of the analysis. In figure 6, we investigate the signature space spanned by a variety of signature channels. The top left panel gives a plot with one signature consisting of events with one lepton and the second signature consisting of events with no leptons. It is seen that the stop patterns (SOPs) that survive the cuts are confined in a small region at the right-bottom corner and have a significant separation from all other mSPs. The panel illustrates the negligible leptonic content in stop decays. The top-right panel is a plot between two signatures where one signature contains a tagged b-jet while the other signature has no tagged b-jets. In this case one finds a significant separation of the CPs and HPs from SUPs and SOPs. The lower-left panel gives a plot where one signature has two tagged b-jets and the other signature has only one tagged b-jet. One again finds that the CPs and HPs are well separated from the SOPs and the SUPs for much the same reason as in upper-right panel. Finally, a plot is given in the lower-right panel where one signature is the average missing P_T while the other signature involves events with no tagged b-jets. Again in this plot the CPs (which include mSP4) and HPs are well separated from the SOPs and SUPs.

The analysis of figure 6 exhibits that for some cases, e.g., for the patterns CP and HP in the upper right hand corner of figure 6, the separation between the SUGRA prediction and the Standard Model background is strikingly clear, allowing for the identification not only of new physics but also of the nature of the pattern that leads to such a signature.

We discuss now the possibility of discriminating sub-patterns within a given pattern class. An analysis illustrating this possibility is given in figure 7. Here the top two panels illustrate how the sub-patterns mSP1, mSP2, mSP4 within the chargino class (CP) are

JHEP04(2008)054

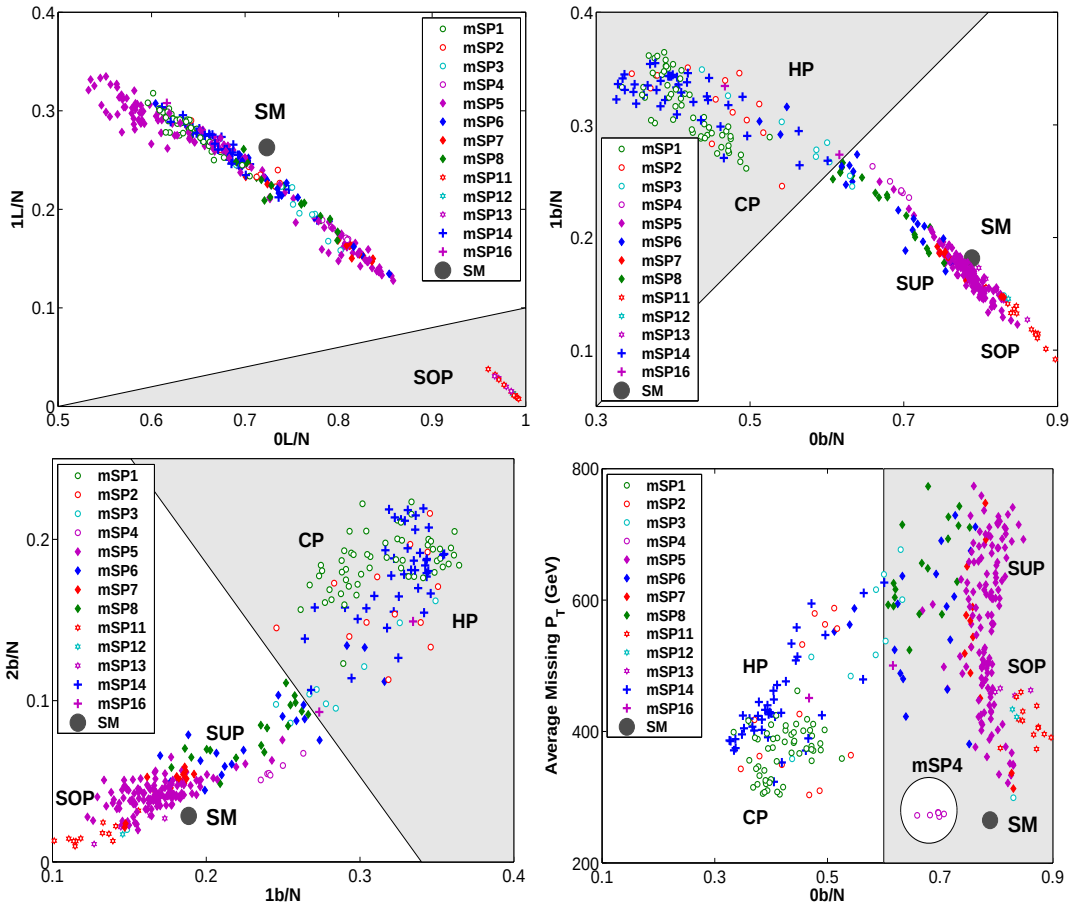

Figure 6: Top Left: An exhibition of the mSPs in the 1L vs 0L where the fraction of events to the total number of events in each case is plotted. The analysis shows that the Stop Patterns (SOP) appearing on the right-bottom corner are easily distinguished from other patterns. The analysis shows that SOP has few lepton signals. Top Right and Bottom Left: Plots in the signature space with fraction of events with 1b vs 0b and 2b vs 1b exhibiting the separation of CPs and HPs from SOPs and SUPs, with CPs and HPs occupying one region, and SOPs and SUPs occupy another in this signature space except for a very small overlap. Bottom Right: An exhibition of the mSPs in the signature space with the average missing P_T for each parameter point in the mSUGRA parameter space along the y-axis and the fraction of events with $0b$ along the x-axis. The plot shows a separation of the CPs and HPs from SOPs and SUPs. Further, mSP4 appears isolated in this plot. Most of the CPs and HPs have less than 60% events without b-jet content. The ratios for the SUSY models refer to the SUSY signal only. The SM point is purely background.

distinguishable with appropriate choice of the signatures. A similar analysis regarding the discrimination for the sub-patterns in the stau class (SUP) is given in the two middle panels. The lower-left panel gives an analysis of how one may discriminate the stop sub-patterns mSP11, mSP12, mSP13 in the stop class (SOP), and finally the lower-right panel shows the plots that allows one to discriminate the Higgs patterns mSP14 and mSP16 from each other. There are a variety of other plots which allow one to discriminate among patterns.

JHEP04(2008)054

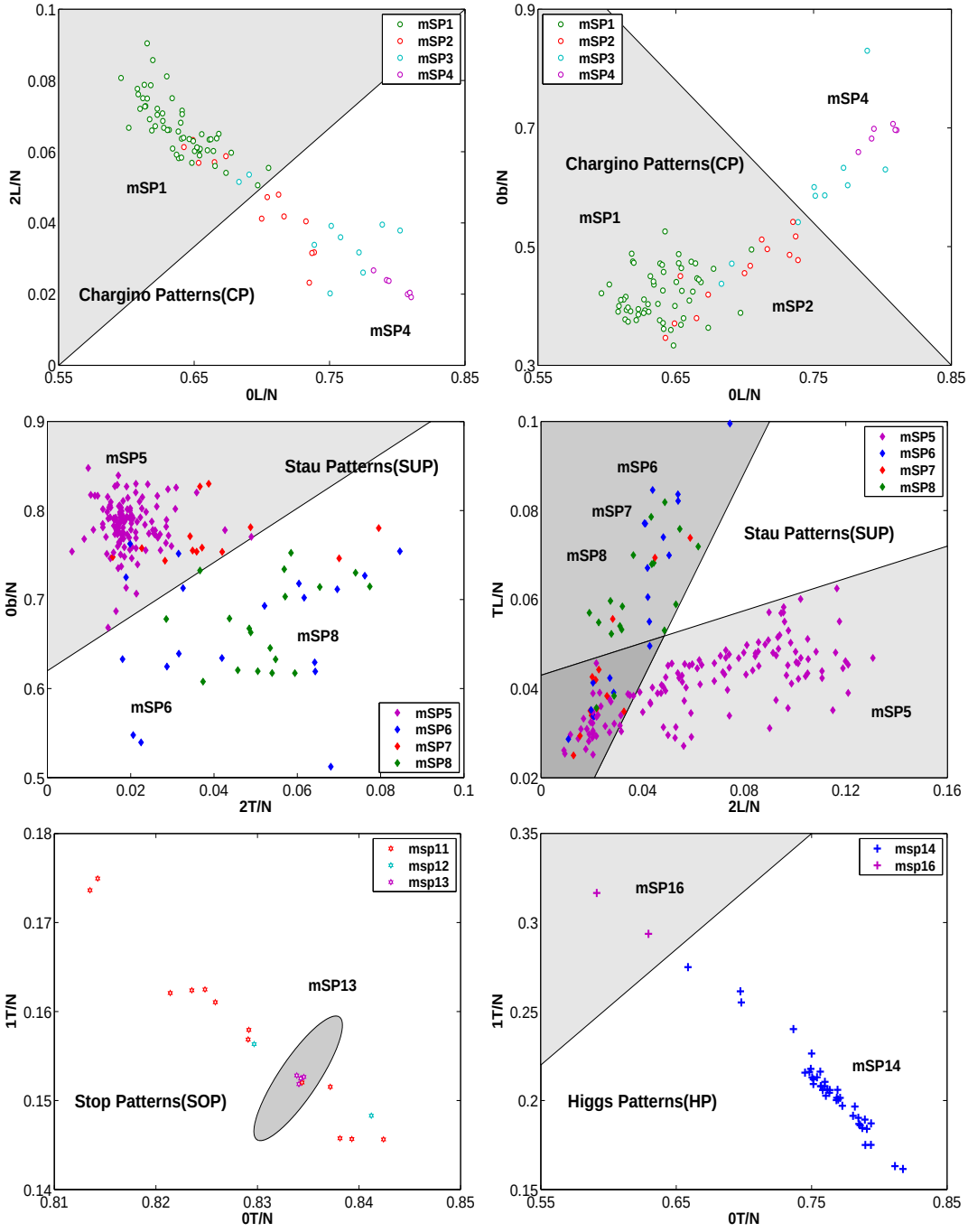

Figure 7: An exhibition of how the mSPs can be discriminated within a given class, i.e., within CPs, SUPs, SOPs, and HPs. The analysis shows that patterns within a given class can be discriminated.

With 40 counting signatures one can have 780 such plots and it is not possible to display all of them. A global analysis where the signatures are simultaneously considered for a large collection of mSPs and NUSPs is discussed in section 4.7.

JHEP04(2008)054

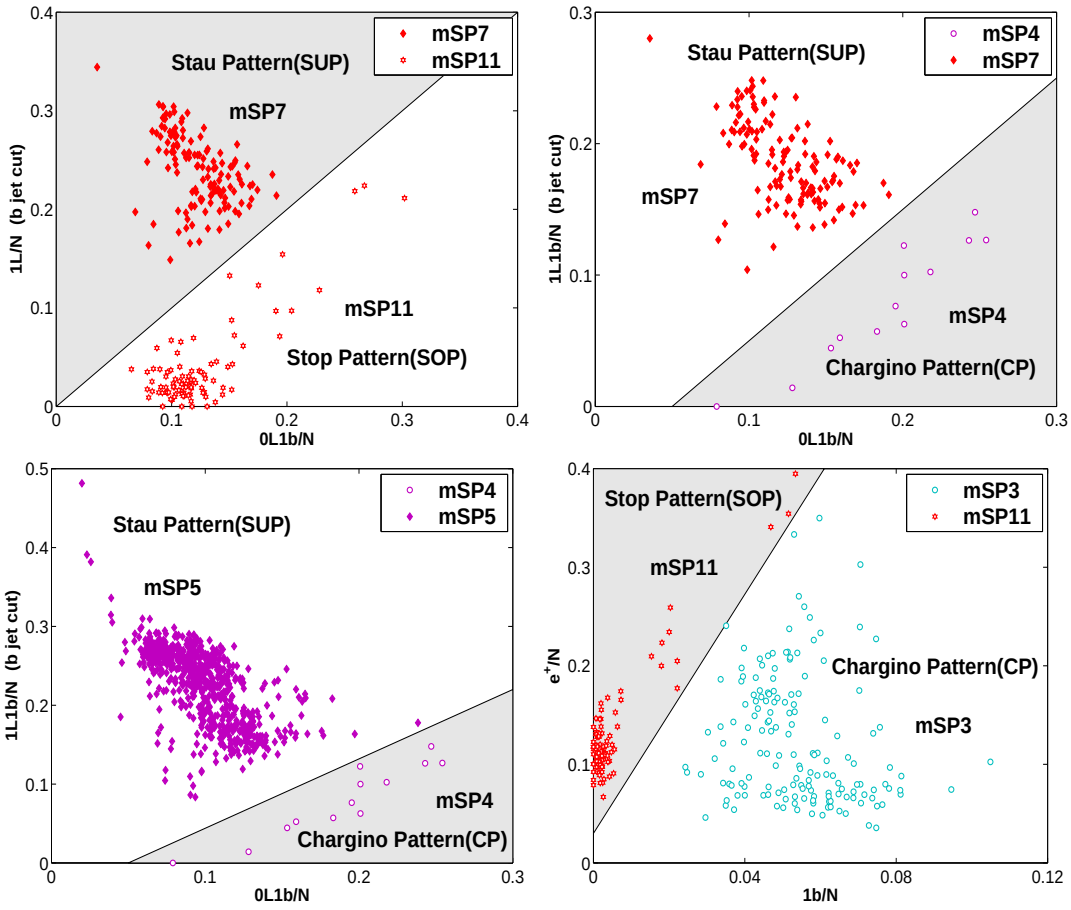

Figure 8: Discrimination among mSPs within both mSUGRA and NUSUGRA models. Two mSPs are presented in each figure in different signature spaces to show the separation for each case. Signals are simulated with constant number of events in PGS4 for each pattern.

As mentioned in the above analysis we have included models which can produce at least 500 SUSY events with 10 fb^{-1} which is lower than our estimated discovery limits for total SUSY events which are about 2200 in this case. The reason for inclusion of points below the discovery limit in the total SUSY events is that some of them can be detected in other channels such as in the trileptonic channel while others will be detectable as the luminosity goes higher. We note in passing that reduction of admissible points makes separation of patterns easier.

4.4 Sparticle signatures including nonuniversalities

In this subsection, we give an analysis including nonuniversalities in three different sectors: NUH, NU3, and NUG. In our analysis we simulate various models with the same constant number of events N which we take as an example to be N= 10^4. To discriminate among the patterns in the signature space, we introduce another set of post trigger cuts, which we denote as 'b jet cuts', in addition to the default post trigger cuts specified in section 4.2.

JHEP04(2008)054

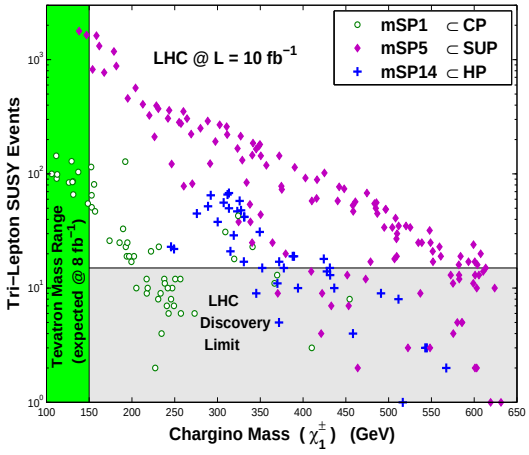

Figure 9: A plot of the number of trilepton events versus the light chargino mass for three patterns, one from each class, CP, SUP and HP. The SUP pattern gives the largest trileptonic signal followed by the HP and CP patterns.

The criteria in the b-jet cuts are the same as the default post trigger cuts, except that we change the condition 'at least two hadronic jets in the event' to 'specifically at least one b-tagged jet in the event'. We exhibit our analysis utilizing both the default cuts and the b jet cuts in figure 8. One can see that even with inclusion of a variety of soft breaking scenarios, some mSPs still have very distinct signatures in some specific channels.

Thus in the top-left panel we give a plot of mSP7 (SUP) and mSP11 (SOP) in the signature space 1L/N (b jet cuts) vs 0L1b/N, where 0L1b/N is obtained with the default post trigger cuts. Here we find that these two model types are clearly distinguishable as highlighted by shaded and unshaded regions. A similar analysis with signatures consisting of 1L1b/N (b jet cuts) vs 0L1b/N for mSP4 (CP) and mSP7 (SUP) is given in the top-right panel. The lower-left panel gives an analysis of mSP4 (CP) and mSP5 (SUP) also in the signature space consisting of 1L1b/N (b jet cuts) vs 0L1b/N. Finally, in the lower-right panel we give an analysis of mSP3 (CP) and mSP11 (SOP) in the signature plane e^+/N vs 1b/N. These analyses illustrate that the patterns and often even the sub-patterns can be discriminated with the appropriate choice of signatures for a general class of SUGRA models including nonuniversalities .

4.5 The trileptonic signal as a pattern discriminant

The trileptonic signal is an important signal for the discovery of supersymmetry. For on-shell decays the trileptonic signal was discussed in the early days in [11, 85] and for off-shell decays in [86]. (For a recent application see [78]). Here we discuss the trileptonic signal in the context of discrimination of hierarchical patterns. In figure 9 we exhibit the dependency of the trilepton signal on the chargino mass. It is seen that mSP5 gives the largest number of events in this channel while the CP pattern (mSP1) and the HP pattern (mSP14) can also produce a large number of trilepton events above the discovery limit, while the chargino mass reach is extended for the mSP5 as opposed to the mSP1

JHEP04(2008)054

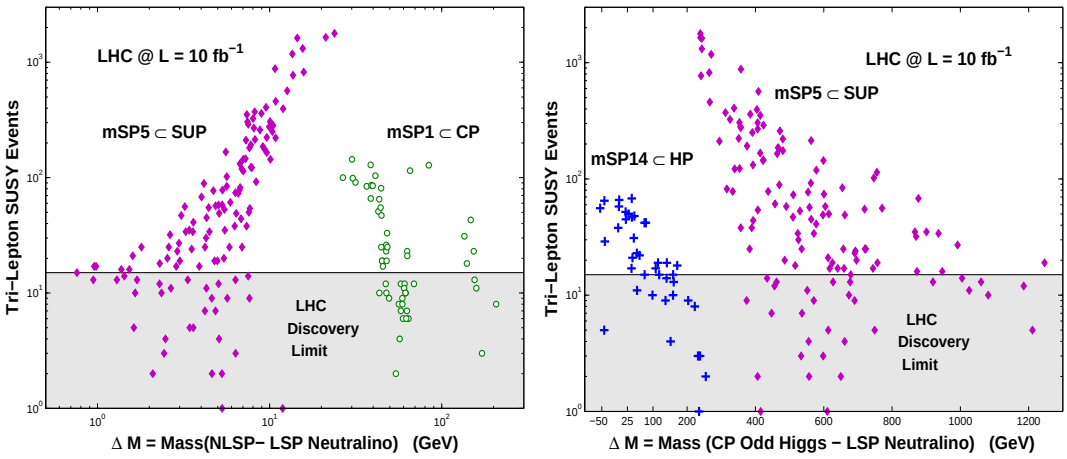

Figure 10: The number of tri-lepton events versus the sparticle mass splittings. The left panel shows clear separations for hierarchical mass patterns in the number of trilepton events produced with 10 fb^{-1} as a function of the NLSP and the LSP mass splitting for the chargino (CP) pattern mSP1 and Stau (SUP) mSP5. The plot on the right shows a similar effect for the case where the mass splitting is taken to be the difference of the CP odd Higgs boson mass and the LSP for both the Higgs pattern mSP14 and the stau pattern mSP5. The Standard Model background is highly suppressed in this channel.

and mSP14. The above observations hold for some of the other SUP patterns as well. Thus the trileptonic signal is strong enough to be probed up to chargino masses of about 600 GeV in the SUP pattern. Another interesting display of the trileptonic signal is when this signal is plotted against some relevant mass splittings. Thus the left-panel of figure 10 gives an analysis for the trileptonic signal for two patterns: the Chargino pattern mSP1 and the Stau pattern mSP5 plotted against the NLSP-LSP mass splitting with 10 fb^{-1} of data. The analysis of the left-panel of figure 10 shows that the SUP pattern presents an excellent opportunity for discovering SUSY through the 3 lepton mode. The analysis also shows a clear separation among mass patterns and further a majority of the model points stand above the discovery limit which in this channel is ≈ 15 events under the post trigger level cuts discussed in section 4.2. The right-panel of figure 10 gives an analysis of the trileptonic signal vs the mass splitting of the CP odd Higgs and the lightest neutralino LSP for patterns mSP5 and mSP14. Again, we see a clear separation of model points. We note that CP odd Higgs can sometimes be even lighter than the LSP, and thus the quantity $\Delta M = M_A - M_{\tilde{\chi}_1^0}$ plotted on the x-axis can sometimes become negative.

4.6 Kinematical distributions

In addition to the event counting signatures discussed above, the kinematical signatures are an important tool for pattern discrimination. We illustrate this using the kinematical variables consisting of missing P_T and the effective mass (see table 6 for their definitions) and an illustration is given in figure 11. Specifically the analysis of figure 11 uses four mSUGRA points one each in the patterns CP, SUP, SOP and HP . The analysis of figure 11

JHEP04(2008)054

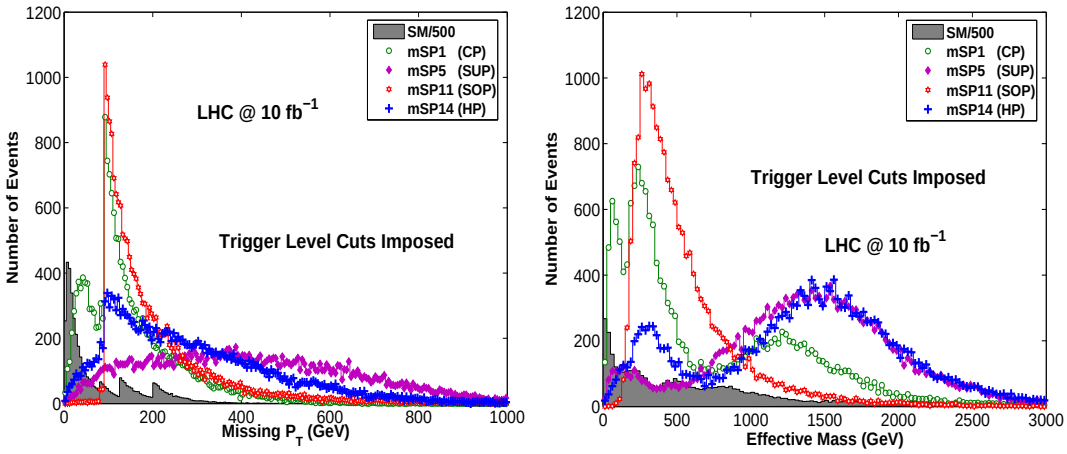

Figure 11: An exhibition of the missing P_T and of the effective mass distributions for 4 different mSUGRA models with each corresponding to one class of mSPs, and for the Standard Model. In the missing P_T distribution as well as in the effective mass distribution, the Standard Model tends to produce events with a lower missing P_T and a lower effective mass relative to the mSUGRA case which generates events at relatively higher missing P_T and effective mass. Further, there is a large variation between different mSUGRA models, as can be seen above. Thus, for example mSP5 (a stau pattern) and mSP14 (a Higgs pattern) have peaks at larger values of missing P_T and larger values of the effective mass relative to mSP1 (a chargino pattern) and mSP11 (a stop pattern). Additionally, the shapes of the distributions are also different. Only trigger level cuts are employed here.

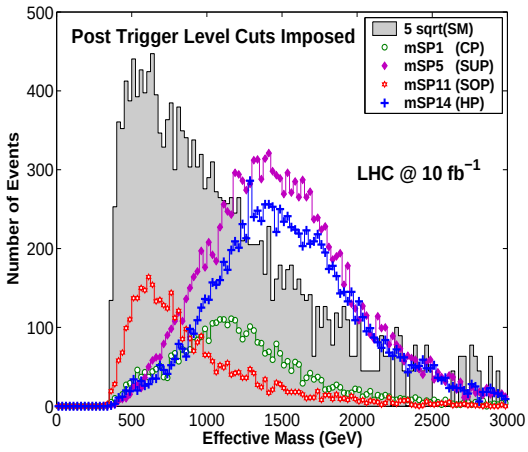

Figure 12: The effective mass distributions for 4 different mSUGRA models with each corresponding to one class of mSPs, and for the Standard Model. Post trigger level cuts are imposed here. The bin size used here is 25 GeV. We exhibit the mSUGRA points used here in the order (m_0, $m_{1/2}$, A_0, $\tan\beta$, signμ): CP (3206.9, 285.3, -1319.8, 9.7, +1), SUP (92.6, 462.1, 352.2, 4.5, +1), SOP (2296.9, 625.0, -5254.9, 13.6, +1), and HP (756.8, 387.0, 1144.9, 56.5, +1).

JHEP04(2008)054

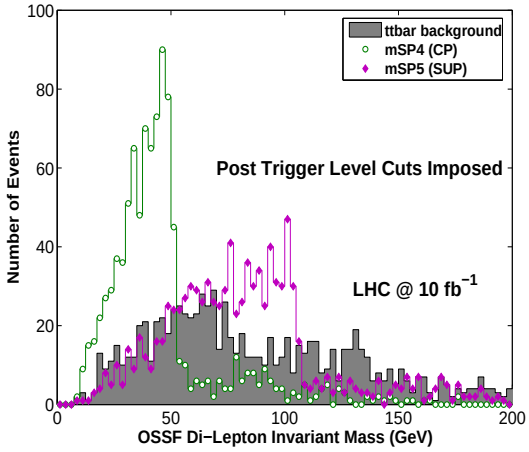

Figure 13: A plot of the opposite sign same flavor (OSSF) di-lepton invariant mass distribution at LHC with $10\,\text{fb}^{-1}$ with the default post trigger cuts imposed for two different mSP points on top of the SM $t\bar{t}$ background. The two mSPs, mSP4 (1674.9, 137.6, 1986.5, 18.6, +1) and mSP5 (84.4, 429.3, -263, 3.4, +1), are clearly distinguishable from each other in the distribution. The mSP4 model point shown here has recently been investigated [87] in the context of helicity amplitudes as a discovery mechanism for supersymmetry.

shows that the distributions for the CP, HP, SOP and SUP are substantially different. It is interesting to note that in the missing P_T distribution, the HP and SUP model points have a relatively flat distribution compared to the CP and SOP model points. The missing P_T distribution and the effective mass distribution are useful when designing post trigger level cuts to optimize the signal over the background. For instance, one can take a 1 TeV effective mass cut to analyze the SUP and HP signals shown in figure 11, but this method will will not work well when it comes to the CP and SOP points since most of their events have a rather small effective mass. To illustrate that different models have different effective mass distributions, and consequently different effective mass cuts are needed for different patterns, an analysis is given in figure 12 for the same set of points in figure 11 with post trigger level cuts imposed.

We also investigate the invariant mass distribution for the opposite sign same flavor (OSSF) di-leptons ($e^+e^-, \mu^+\mu^-$) in figure 13. We applied the default post trigger cuts as in section 4.2 to suppress the SM background. As a comparison the dominant Standard Model $t\bar{t}$ background is also exhibited. We have cross checked our work with the CMS Note [76], and found good agreement regarding the SUSY signals and the Standard Model background. It is seen that the two mSP points plotted in figure 13 are easily distinguishable from each other.

4.7 A 'global' analysis, fuzzy signature vectors, and pattern discrimination

In the above we have given specific examples of how patterns can be differentiated from each other. In the previous sections we used only a few of the 40 signatures exhibited in table 6. However, in the analysis we have carried out we have examined all of them.

JHEP04(2008)054

Thus for each parameter point we have analyzed 40 signatures. We now define correlations among these signatures. Thus consider an ordered set where the signatures are labeled $S_1, S_2, \ldots, S_{40}$ and let the number of events in each signature be $N_1, N_2, \ldots, N_{40}$. Define a signature vector for a given point x_α ($\alpha = 1, 2, \ldots, p$) in the parameter space

$$\xi^a = (\xi^a_1, \xi^a_2, \ldots, \xi^a_{40}) \tag{4.1}$$

where $\xi_i = N^a_i/N$ and N is the total number of SUSY events. As the parameter point x_α varies over the allowed range within a given pattern it generates a signature vector where the elements trace out a given range. Thus for a pattern X one generates a fuzzy pattern vector $\Delta\xi^X$ so that

$$\Delta\xi^X = (\Delta\xi^X_1, \Delta\xi^X_2, \ldots, \Delta\xi^X_{40}), \tag{4.2}$$

where $\Delta\xi^X_i$ is the range traced out by the element ξ^X_i as the parameter point x_α moves in the allowed parameter space of the pattern X. What makes the vector $\Delta\xi^X$ fuzzy is that its elements are not single numbers but a set which cover a range. We define now the inner product of two such fuzzy pattern vectors so that

$$C_{XY} \equiv (\Delta\xi^X | \Delta\xi^Y) = 0(1) \tag{4.3}$$

where the inner product is 0 if the element $\Delta\xi^X_i$ and $\Delta\xi^Y_i$ overlap for all i ($i = 1, ., 40$), and 1 if at least one of the elements of pattern X, $\Delta\xi^X_j$ does not overlap with $\Delta\xi^Y_j$, the element for pattern Y. Therefore, if for two patterns X and Y one finds there is no overlap at least for one signature component $\Delta\xi_j$, then these two patterns can be distinguished in this specific signature and one obtains $C_{XY} = 1$. Otherwise $C_{XY} = 0$ which means that all components of $\Delta\xi^X$ and $\Delta\xi^Y$ have an overlap and cannot be distinguished under this critera. We can generalize the above procedure for the signatures

$$\zeta_{i,j} = \frac{N_i}{N_j}, \quad (i, j = 1, \ldots, 40). \tag{4.4}$$

Repeating the previous analysis, one can construct another fuzzy signature vector for pattern X as

$$\Delta\zeta^X = (\Delta\zeta^X_{1,2}, \ldots, \Delta\zeta^X_{i,j}, \ldots, \Delta\zeta^X_{39,40}) \tag{4.5}$$

where the elements have a range corresponding to the range spanned by the soft parameters x_α as they move over the parameter space specific to the pattern. Further, the definition of the inner product eq. (4.3) still holds for this new fuzzy signature vector. We have carried out a full signature analysis of such comparisons, using 40 different signatures, and their combinations as defined in eq. (4.4) and eq. (4.5). An illustration of the global analysis is given in figure 14. The analysis shows that it is possible to often distinguish patterns using the criterion of eq. (4.3). We note that the analyses exhibited in figure 8 are the special cases of the results in figure 14. For instance, the clear separation between mSP7 and mSP11 in the signature space shown in the top-left panel of figure 8 gives the elements $C_{45} = C_{54} = 1$ of figure 14. As emphasized already the analysis of figure 14 is for illustrative

M-Pattern	mSP5	mSP1	mSP3	mSP7	mSP11	mSP6	mSP12	mSP13	NUSP1	mSP4	mSP18	NUSP13	mSP20	mSP10	mSP17	NUSP3	mSP19	NUSP5	NUSP8	NUSP10	NUSP4	NUSP9	M-Pattern
mSP5	0	0	0	0	1	0	1	1	0	1	0	1	1	1	0	1	1	1	1	1	0	1	mSP5
mSP1	0	0	0	0	0	0	1	0	0	1	0	1	1	1	0	0	1	1	1	1	0	1	mSP1
mSP3	0	0	0	0	1	0	1	1	0	0	0	1	1	1	1	0	1	1	1	1	1	1	mSP3
mSP7	0	0	0	0	1	0	1	1	0	1	0	1	1	1	1	0	1	1	1	1	0	1	mSP7
mSP11	1	0	1	1	0	0	1	1	1	0	1	1	1	1	1	1	1	1	1	1	1	1	mSP11
mSP6	0	0	0	0	0	0	1	0	0	0	0	1	1	1	0	0	1	1	1	1	0	1	mSP6
mSP12	1	1	1	1	1	1	0	0	1	1	1	1	1	1	1	1	1	1	1	1	1	1	mSP12
mSP13	1	0	1	1	1	0	0	0	1	1	0	1	1	1	1	1	1	1	1	1	1	1	mSP13
NUSP1	0	0	0	0	1	0	1	1	0	1	1	1	1	1	1	1	1	1	1	1	1	1	NUSP1
mSP4	1	1	0	1	0	0	1	1	1	0	1	1	1	1	1	1	1	1	1	1	1	1	mSP4
mSP18	0	0	0	0	1	0	1	0	1	1	0	1	1	1	1	1	1	1	1	1	1	1	mSP18
NUSP13	1	1	1	1	1	1	1	1	1	1	1	0	1	1	1	1	1	1	1	1	1	1	NUSP13
mSP20	1	1	1	1	1	1	1	1	1	1	1	1	0	1	1	1	1	1	1	1	1	1	mSP20
mSP10	1	1	1	1	1	1	1	1	1	1	1	1	1	0	1	1	1	1	1	1	1	1	mSP10
mSP17	0	0	1	1	1	0	1	1	1	1	1	1	1	1	0	1	1	1	1	1	1	1	mSP17
NUSP3	1	0	0	0	1	0	1	1	1	1	1	1	1	1	1	0	1	1	1	1	1	1	NUSP3
mSP19	1	1	1	1	1	1	1	1	1	1	1	1	1	1	1	1	0	1	1	1	1	1	mSP19
NUSP5	1	1	1	1	1	1	1	1	1	1	1	1	1	1	1	1	1	0	1	1	1	1	NUSP5
NUSP8	1	1	1	1	1	1	1	1	1	1	1	1	1	1	1	1	1	1	0	1	1	1	NUSP8
NUSP10	1	1	1	1	1	1	1	1	1	1	1	1	1	1	1	1	1	1	1	0	1	1	NUSP10
NUSP4	0	0	1	0	1	0	1	1	1	1	1	1	1	1	1	1	1	1	1	1	0	1	NUSP4
NUSP9	1	1	1	1	1	1	1	1	1	1	1	1	1	1	1	1	1	1	1	1	1	0	NUSP9
M-Pattern	mSP5	mSP1	mSP3	mSP7	mSP11	mSP6	mSP12	mSP13	NUSP1	mSP4	mSP18	NUSP13	mSP20	mSP10	mSP17	NUSP3	mSP19	NUSP5	NUSP8	NUSP10	NUSP4	NUSP9	M-Pattern

Figure 14: A table exhibiting the discrimination of patterns using the criterion of eq. (4.3) where various signatures with both the default post trigger cuts and b jet cuts are utilized. If the element of i^{th} row and j^{th} column is 1, i.e., $C_{ij} = 1$, one can distinguish the i^{th} mass pattern from the j^{th} one.

purposes as we used a random sample of 22 patterns out of 37. Inclusion of each additional mass pattern brings in a significant set of model points which need to be simulated, and here one is limited by computing power. The full analysis including all the patterns can be implemented along similar lines with the necessary computing power. Finally we note that the analysis in figure 14 is done without statistical uncertainties. Inclusion of uncertainties in pattern analysis would certainly be worthwhile in a future work.

5. Signature degeneracies and resolution of soft parameters

5.1 Lifting signature degeneracies

It may happen that two distinct points in the soft parameter space may lead to the same set of signatures for a given integrated luminosity within some predefined notion of indistinguishability. Thus consider two parameter points A and B and define the 'pulls' in each of their signatures by

$$P_i = \frac{|n_i^A - n_i^B|}{\sigma_{AB}},$$
$$\sigma_{AB} = \sqrt{(\delta n_i^A)^2 + (\delta n_i^B)^2 + (\delta n_i^{SM})^2}. \tag{5.1}$$

Here $\delta n_i^A \sim \sqrt{n_i^A}$ is the uncertainty in the signature events n_i^A, and we estimate the

JHEP04(2008)054

i	S_i	A	B	P_i	A'	B'	P_i	A	B	P_i	A'	B'	P_i
0	N	743	730	0.3	878	817	1.2	35947	35948	0.0	45479	41135	12.1
1	0L	430	414	0.4	484	437	1.3	20771	20592	0.7	25897	23427	9.1
2	1L	221	230	0.3	294	271	0.8	10641	10676	0.2	13669	12414	6.3
3	2L	78	71	0.5	83	96	0.8	3745	3933	1.8	4904	4369	4.5
4	3L	10	13	0.5	16	11	0.8	703	691	0.3	927	830	1.9
5	4L	4	2	0.6	1	2	0.4	87	56	2.1	82	95	0.8
6	0T	620	610	0.2	731	674	1.2	29533	30220	2.3	38213	34138	12.4
7	1T	112	104	0.4	137	129	0.4	5722	5140	4.6	6528	6296	1.7
8	2T	11	14	0.5	10	14	0.7	643	541	2.4	693	659	0.8
9	3T	0	2	1.1	0	0	0.0	44	45	0.1	43	40	0.3
10	4T	0	0	0.0	0	0	0.0	5	2	0.9	2	2	0.0
11	TL	38	26	1.2	50	45	0.4	1779	1597	2.6	2069	2029	0.5
12	OS	59	57	0.2	66	70	0.3	2755	2927	1.9	3665	3285	3.7
13	SS	19	14	0.7	17	26	1.1	990	1006	0.3	1239	1084	2.6
14	OSSF	40	46	0.5	49	52	0.2	2023	2112	1.1	2710	2389	3.7
15	SSSF	7	9	0.4	10	13	0.5	458	452	0.2	537	481	1.4
16	OST	7	8	0.2	5	9	0.9	400	345	1.6	428	402	0.7
17	SST	4	6	0.5	5	5	0.0	243	196	1.8	265	257	0.3
18	0L1b	50	59	0.7	61	56	0.4	2586	2710	1.4	3527	3387	1.4
19	1L1b	45	39	0.5	48	53	0.4	1767	1799	0.4	2431	2268	1.9
20	2L1b	9	8	0.2	15	21	0.8	648	674	0.6	853	778	1.5
21	0T1b	86	88	0.1	100	110	0.6	4099	4357	2.3	5734	5353	3.0
22	1T1b	21	15	0.8	22	20	0.3	923	836	1.7	1150	1106	0.8
23	2T1b	3	3	0.0	4	2	0.6	115	109	0.3	111	129	0.9
24	0L2b	20	20	0.0	12	13	0.2	608	685	1.7	890	838	1.0
25	1L2b	11	12	0.2	15	24	1.2	476	474	0.1	625	598	0.6
26	2L2b	3	5	0.6	1	2	0.4	175	190	0.6	251	227	0.9
27	0T2b	30	29	0.1	25	32	0.8	1027	1115	1.6	1481	1379	1.6
28	1T2b	4	6	0.5	4	6	0.5	242	234	0.3	300	297	0.1
29	2T2b	0	2	1.1	0	1	0.7	30	40	1.0	28	27	0.1
30	ep	71	71	0.0	93	83	0.6	3240	3219	0.2	4251	3957	2.6
31	em	47	44	0.3	52	51	0.1	2055	1994	0.8	2618	2358	3.0
32	mp	60	70	0.7	103	78	1.5	3338	3442	1.0	4236	3821	3.8
33	mm	43	45	0.2	46	59	1.0	2008	2021	0.2	2564	2278	3.4
34	tp	60	53	0.5	69	80	0.7	3203	2803	4.2	3564	3504	0.6
35	tm	52	51	0.1	68	49	1.4	2519	2337	2.1	2964	2792	1.9
36	0b	597	585	0.3	717	642	1.7	29276	29072	0.7	36432	32602	11.9
37	1b	110	107	0.2	126	132	0.3	5150	5314	1.3	7003	6593	2.9
38	2b	34	37	0.3	29	39	1.0	1302	1389	1.4	1810	1706	1.4
39	3b	1	1	0.0	6	2	1.1	192	153	1.7	215	205	0.4
40	4b	1	0	0.7	0	2	1.1	27	20	0.8	19	29	1.2

Table 7: An exhibition of lifting the degeneracy of two points in the mSUGRA parameter space using luminosity. Two pairs of points (A, B) and (A', B') are indistinguishable under the 2 sigma criteria at 10 fb^{-1} luminosity (column 3-8), but can be clearly separated when the luminosity increases to 500 fb^{-1} (column 9-14). The Standard Model uncertainty is estimated as $\delta n_i^{SM} = (\delta n_i^A + \delta n_i^B)/2$.

SM uncertainty as $\delta n_i^{SM} \sim \sqrt{y}(\delta n_i^A + \delta n_i^B)/2$. Here the parameter y parameterizes the effect of the SM events, and for the analysis in this section, we take $y = 1$. In other words, if the pulls in each of the signatures is less than 5, then the two SUGRA parameter space points are essentially indistinguishable in the signature space. In such a situation one could still distinguish model points either by including more signatures, or by an

JHEP04(2008)054

increase in luminosity. Thus, for example, inclusion of the Higgs production cross sections, $B_s \to \mu^+\mu^-$ constraints, as well as the inclusion of neutralino proton scattering cross sections constraints tend to discriminate among the model parameter points as shown in ref. [2]. Here we point out that in some cases increasing the luminosity can allow one to lift the degeneracies enhancing a subset of signatures in one case relative to the other. For illustration we consider the following two sets of points in the pattern mSP5 in the mSUGRA parameter space in the following order (m_0, $m_{1/2}$, A_0, $\tan\beta$, signμ).

$$\begin{array}{l} \text{Point A } (192.6, 771.3,\ 1791.1, 8.8, +1), \\ \text{Point B } (163.0, 761.3, -775.8, 4.7, +1); \end{array} \tag{5.2}$$

$$\begin{array}{l} \text{Point A}' \ (159.3, 732.3, -783.1, 5.6, +1), \\ \text{Point B}' \ (163.5, 753.3, -918.2, 3.3, +1). \end{array} \tag{5.3}$$

In table 7 we compare the pulls for the pairs of points (A, B) and (A', B') at an integrated luminosity of 10 fb^{-1} and 500 fb^{-1}. For points A and B, one finds that the pulls are all less than 2 for an integrated luminosity of 10 fb^{-1}. However, for an integrated luminosity of 500 fb^{-1}, the pulls for signatures $(6, 7, 8, 11, 21, 34)$ increase significantly and the pull for signature number 7 is in excess of 4.5 allowing one to discriminate between the two parameter points A and B. A very similar analysis is carried out for parameter points A' and B'. Here one finds that the signature $(0, 1, 2, 3, 6, 12, 14, 32, 33, 36)$ receive a big boost as we go from 10 fb^{-1} to 500 fb^{-1}, and the signatures $(0, 1, 2, 6, 36)$ give pulls greater than 5, with the largest pulls being in excess of 12, allowing one to discriminate between the parameter points A' and B'. We note the analysis ignores systematic errors and also does not consider an ensemble of simulations. Nonetheless it does illustrate the effects of moving from a low to a high LHC luminosity allowing one to discriminate some model pairs, which appear degenerate in the signature space at one luminosity, but can become distinct from each other at a larger luminosity.

5.2 Resolving soft parameters using LHC data

We discuss now the issue of how well we can resolve the points in the parameter space x_α ($\alpha = 1, \ldots, p$) for a given luminosity. Consider eq. (5.1) and set $\delta N = \sqrt{N}$, and parameterize the standard model uncertainty by $\delta N^{SM} = \sqrt{y}\delta N$. Next we set the criterion for the resolution of two adjacent points in the SUGRA parameter space separated by Δx_α so that the separation in the signature space satisfies

$$\frac{\Delta N}{\sqrt{2N + yN}} = 5. \tag{5.4}$$

Since $N = \sigma_{\rm susy}(x_\alpha)\mathcal{L}_{\rm LHC}$, where $\sigma_{\rm susy}$ is the cross section for the production of sparticles, and $\mathcal{L}_{\rm LHC}$ is the LHC integrated luminosity, the resolution achievable in the vicinity of SUGRA parameter point x_α at that luminosity is given by

$$\Delta x_\alpha = \frac{5}{2}(2+y)^{1/2}\mathcal{L}_{\rm LHC}^{-1/2}\left(\frac{\partial\sigma_{\rm susy}^{1/2}(x)}{\partial x_\alpha}\right)^{-1}. \tag{5.5}$$

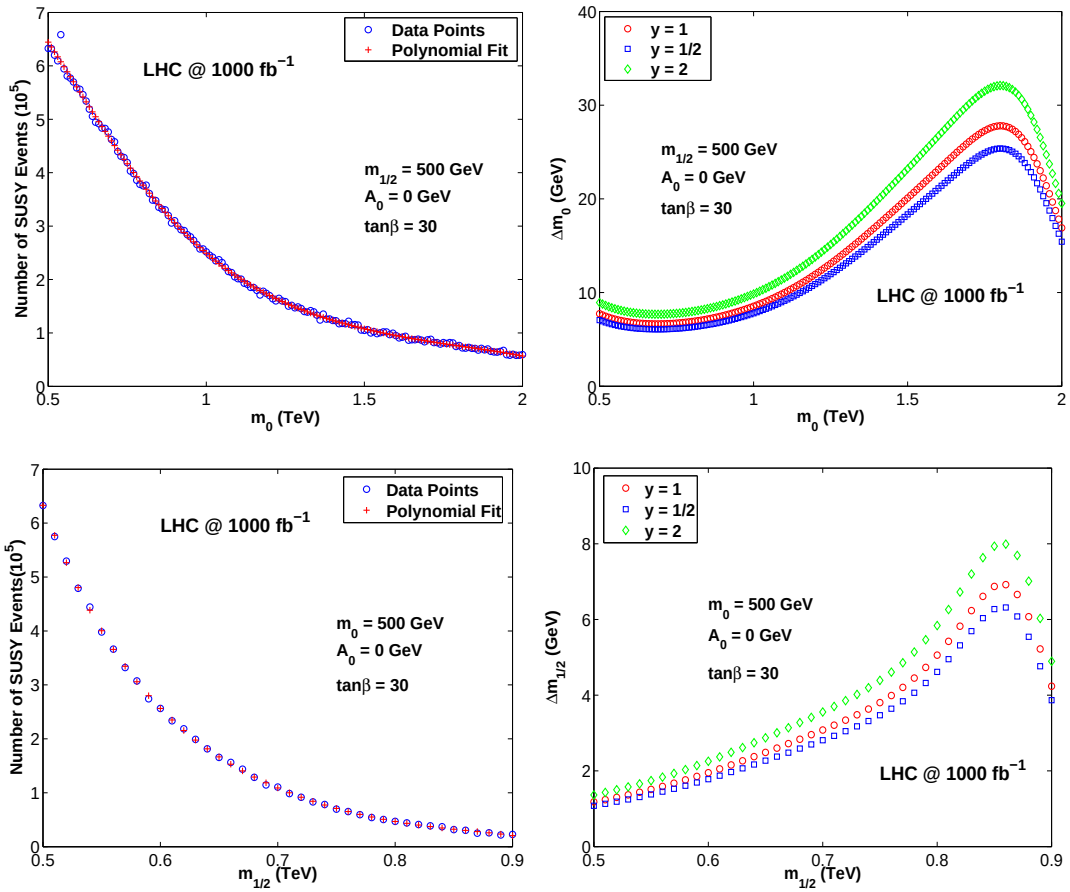

Figure 15: An analysis showing the resolutions in m_0 and $m_{1/2}$ that can be reached with 1000 fb^{-1} of integrated luminosity under the REWSB constraints. The two left panels give the number of SUSY events vs m_0 (top left panel) and vs $m_{1/2}$ (lower left panel) for 1000 fb^{-1} of integrated luminosity. The right panels give the resolutions in m_0 (top right panel) and in $m_{1/2}$ (lower right panel) using the left panels.

In figure 15 we give an illustration of the above when m_0 varies between 500 GeV and 2000 GeV while $m_{1/2} = 500$ GeV, $A_0 = 0, \tan\beta = 30$, and $\mu > 0$. From figure 15 one finds that the resolution in m_0 strongly depends on the point in the parameter space and on the luminosity. Quite interestingly a resolution as small as a few GeV can be achieved for m_0 in the range 500-1000 GeV with 1000 fb^{-1} of integrated luminosity. A similar analysis varying $m_{1/2}$ in the range 500–900 GeV for the case when $m_0 = 500$ GeV, $A_0 = 0, \tan\beta = 30$ and $\mu > 0$, shows that a resolution in $m_{1/2}$ as low as 1 GeV can be achieved with 1000 fb^{-1} of integrated luminosity.

6. Conclusion

The minimal supersymmetric Standard Model has 32 sparticle masses. Since the soft breaking sector MSSM is arbitrary, one is led to a landscape of as many as 10^{28} or more

JHEP04(2008)054

possibilities for the sparticle mass hierarchies. The number of possibilities is drastically reduced in well motivated models such as supergravity models, and one expects similar reductions to occur also in gauge and anomaly mediated models, and in string and brane models. In this work we have analyzed the mass hierarchies for the first four lightest sparticle (aside from the lightest Higgs boson) for supergravity models. Specifically, in section 2 we analyzed the mass hierarchies for the mSUGRA model and for supergravity models with nonuniversalities in the soft breaking in the Higgs sector, nonuniversalities in the soft breaking in the third generation sector, and nonuniversalities in the soft breaking in the gaugino sector. It is found that in each case only a small number of mass hierarchies or patterns survive the rigorous constraints of radiative breaking of the electroweak symmetry, relic density constraints on cold dark matter from the WMAP data, and other experimental constraints from colliders. These mass hierarchies can be conveniently put into different classes labeled by the sparticle which is next heavier after the LSP. For the SUGRA models we find six different classes: chargino patterns, stau patterns, stop patterns, Higgs patterns, neutralino patterns, and gluino patterns. Benchmarks for each of these patterns were given in section 3. In section 4 we discussed the techniques for the analysis of the signatures and the technical details on simulations of sparticle events. In this section we also discuss the backgrounds to the SUSY phenomena arising from the Standard Model processes. Additionally we discussed here the identification of patterns based on 40 event identification criteria listed in figure 14. It is found that these criteria allow one to discriminate among most of the patterns. An analysis of how one may lift degeneracies in the signature space, and how accurately one can determine the soft parameters using the LHC luminosities is given in section 5. It is hoped that the analysis of the type discussed here would help not only in the search for supersymmetry but also allow one to use the signatures to extrapolate back to the underlying supersymmetric model using the experimental data when such data from the LHC comes in. In the above our analysis was focused on supergravity unified models. However, the techniques discussed here have a much wider applicability to other models, including models based on gauge and anomaly mediated breaking, as well as string and brane based models.

Acknowledgments

This work is supported in part by NSF grant PHY-0456568. Some of the results given here were presented at the workshop "LHC New Physics Signatures Workshop", at the Michigan Center for Theoretical Physics, January 5-11, 2008, and at the conference "From Strings to LHC-II", Bangalore, December 19-23, 2007. The authors have benefited from interactions at these workshops.

JHEP04(2008)054

A. Benchmarks for sparticle mass hierarchies

Chargino Patterns (CPs)

SUGRA Pattern	m_0 (GeV)	$m_{1/2}$ (GeV)	A_0 (GeV)	$\tan\beta$ (v_u/v_d)	μ (sign)	NUH $(\delta_{H_u}, \delta_{H_d})$	NU3 $(\delta_{q3}, \delta_{tbR})$	NUG $(\delta_{M_2}, \delta_{M_3})$
mSP1	2001	411	0	30.0	+	(0,0)	(0,0)	(0,0)
mSP1	2366	338	-159	9.8	-	(0,0)	(0,0)	(0,0)
mSP1	1872	327	-1893	14.9	+	(0.107,0.643)	(0,0)	(0,0)
mSP1	1041	703	1022	11.6	+	(0,0)	(-0.524,-0.198)	(0,0)
mSP1	1361	109	1058	14.4	+	(0,0)	(0,0)	(0.929,0.850)
mSP2	1125	614	2000	50.0	+	(0,0)	(0,0)	(0,0)
mSP2	2365	1395	3663	42.2	-	(0,0)	(0,0)	(0,0)
mSP2	1365	595	3012	35.1	+	(0.116,-0.338)	(0,0)	(0,0)
mSP2	1166	507	-954	59.6	+	(0,0)	(0.325,0.458)	(0,0)
mSP2	1414	221	-551	54.3	+	(0,0)	(0,0)	(0.156,0.968)
mSP3	741	551	0	50.0	+	(0,0)	(0,0)	(0,0)
mSP3	1585	1470	3133	39.1	-	(0,0)	(0,0)	(0,0)
mSP3	694	674	-1564	27.0	+	(0.922,-0.293)	(0,0)	(0,0)
mSP3	570	559	1042	41.3	+	(0,0)	(-0.482,-0.202)	(0,0)
mSP3	392	312	320	41.3	+	(0,0)	(0,0)	(-0.404,0.908)
mSP4	1674	137	1985	18.6	+	(0,0)	(0,0)	(0,0)
mSP4	1824	127	-1828	6.4	-	(0,0)	(0,0)	(0,0)
mSP4	1021	132	-638	6.6	+	(0,0)	(-0.020,0.963)	(0,0)
mSP4	2181	127	-3859	3.9	+	(0,0)	(0,0)	(0.836,-0.248)
NUSP1	2738	1689	-4243	42.4	+	(0,0)	(-0.828,-0.899)	(0,0)
NUSP1	540	1190	2516	13.9	+	(0,0)	(0,0)	(-0.408,-0.660)
NUSP2	845	726	-75	48.4	+	(0,0)	(-0.694,-0.400)	(0,0)
NUSP3	396	1018	-179	18.3	+	(0,0)	(0,0)	(0.250,-0.452)
NUSP4	400	1558	2511	5.9	+	(0,0)	(0,0)	(-0.401,-0.607)

Table 8: Benchmarks for the class CP where the chargino $\widetilde{\chi}_1^{\pm}$ is the NLSP in mSUGRA and in NUSUGRA models. Benchmarks are computed with ${m_b}^{\overline{\rm MS}}(m_b) = 4.23$ GeV, ${\alpha_s}^{\overline{\rm MS}}(M_Z) = .1172$, and $m_t(\text{pole}) = 170.9$ GeV with SuSpect 2.34 interfaced to micrOMEGAS 2.07.

Gluino Patterns (GPs)

SUGRA Pattern	m_0 (GeV)	$m_{1/2}$ (GeV)	A_0 (GeV)	$\tan\beta$ (v_u/v_d)	μ (sign)	NUH $(\delta_{H_u}, \delta_{H_d})$	NU3 $(\delta_{q3}, \delta_{tbR})$	NUG $(\delta_{M_2}, \delta_{M_3})$
NUSP13	2006	1081	-2027	21.1	+	(0,0)	(0,0)	(0.207,-0.844)
NUSP14	3969	1449	-6806	29.3	+	(0,0)	(0,0)	(0.611,-0.834)
NUSP15	1387	695	2781	50.5	+	(0,0)	(0,0)	(0.136,-0.827)

Table 9: Benchmarks for the class GP where the gluino $\widetilde{g}$ is the NLSP. Such a pattern was only seen to appear in NUSUGRA models with non universal gaugino masses.

JHEP04(2008)054

Stau Patterns (SUPs)

SUGRA Pattern	m_0 (GeV)	$m_{1/2}$ (GeV)	A_0 (GeV)	$\tan\beta$ (v_u/v_d)	μ (sign)	NUH $(\delta_{H_u}, \delta_{H_d})$	NU3 $(\delta_{q3}, \delta_{tbR})$	NUG $(\delta_{M_2}, \delta_{M_3})$
mSP5	111	531	0	5.0	+	(0,0)	(0,0)	(0,0)
mSP5	162	569	1012	15.8	-	(0,0)	(0,0)	(0,0)
mSP5	191	545	-722	17.2	+	(-0.340,-0.332)	(0,0)	(0,0)
mSP5	114	440	-50	15.2	+	(0,0)	(-0.204,-0.846)	(0,0)
mSP5	75	348	301	12.0	+	(0,0)	(0,0)	(0.234,-0.059)
mSP6	245	370	945	31.0	+	(0,0)	(0,0)	(0,0)
mSP6	1452	1651	2821	38.5	-	(0,0)	(0,0)	(0,0)
mSP6	356	545	927	31.7	+	(0.667,0.055)	(0,0)	(0,0)
mSP6	442	463	1150	41.0	+	(0,0)	(-0.187,-0.546)	(0,0)
mSP6	308	307	965	35.6	+	(0,0)	(0,0)	(-0.383,0.405)
mSP7	75	201	230	14.0	+	(0,0)	(0,0)	(0,0)
mSP7	781	1423	983	36.8	-	(0,0)	(0,0)	(0,0)
mSP7	428	671	484	43.8	+	(-0.392,-0.808)	(0,0)	(0,0)
mSP7	226	426	944	27.1	+	(0,0)	(0.176,-0.430)	(0,0)
mSP7	143	425	266	23.4	+	(0,0)	(0,0)	(0.718,0.100)
mSP8	1880	877	4075	54.8	+	(0,0)	(0,0)	(0,0)
mSP8	994	1073	3761	38.1	-	(0,0)	(0,0)	(0,0)
mSP8	602	684	805	49.6	+	(0.490,0.326)	(0,0)	(0,0)
mSP8	470	624	-88	55.4	+	(0,0)	(-0.531,-0.075)	(0,0)
mSP8	525	450	642	56.4	+	(0,0)	(0,0)	(0.623,0.246)
mSP9	667	1154	-125	51.0	+	(0,0)	(0,0)	(0,0)
mSP9	560	1156	-1092	39.5	-	(0,0)	(0,0)	(0,0)
mSP9	362	602	268	37.0	+	(0.969,-0.232)	(0,0)	(0,0)
mSP9	496	731	679	49.3	+	(0,0)	(-0.241,-0.452)	(0,0)
mSP9	485	478	-128	52.8	+	(0,0)	(0,0)	(0.971,0.653)
mSP10	336	772	-3074	10.8	+	(0,0)	(0,0)	(0,0)
mSP10	738	1150	-4893	15.5	+	(0,0)	(0.802,0.343)	(0,0)
mSP17	908	754	5123	25.4	-	(0,0)	(0,0)	(0,0)
mSP18	344	686	-2718	13.8	-	(0,0)	(0,0)	(0,0)
mSP18	322	806	-3069	9.3	+	(0.526,-0.707)	(0,0)	(0,0)
mSP18	60	290	-339	5.2	+	(0,0)	(0,0)	(0.967,-0.074)
mSP19	1530	1875	13081	16.3	-	(0,0)	(0,0)	(0,0)
mSP19	1828	1326	-5102	32.3	+	(0.592,-0.213)	(0,0)	(0,0)
mSP19	782	637	2688	37.9	+	(0,0)	(0,0)	(0.451,-0.551)
NUSP5	649	955	-1984	33.5	+	(0,0)	(-0.763,0.701)	(0,0)
NUSP6	1360	1736	-2871	46.1	+	(0,0)	(-0.466,0.694)	(0,0)
NUSP7	1481	1531	-3169	42.2	+	(0,0)	(0,0)	(0.117,-0.463)
NUSP8	670	1788	371	57.9	+	(0,0)	(0,0)	(-0.223,0.931)
NUSP9	46	1938	-48	13.0	+	(0,0)	(0,0)	(-0.412,-0.650)

Table 10: Benchmarks for the class SUP where the stau $\widetilde{\tau}_1$ is the NLSP in mSUGRA and in NUSUGRA.

Stop Patterns (SOPs)

SUGRA Pattern	m_0 (GeV)	$m_{1/2}$ (GeV)	A_0 (GeV)	$\tan\beta$ (v_u/v_d)	μ (sign)	NUH $(\delta_{H_u}, \delta_{H_d})$	NU3 $(\delta_{q3}, \delta_{tbR})$	NUG $(\delta_{M_2}, \delta_{M_3})$
mSP11	871	1031	-4355	10.0	+	(0,0)	(0,0)	(0,0)
mSP11	1653	909	7574	5.9	-	(0,0)	(0,0)	(0,0)
mSP11	1391	1089	8192	14.9	+	(0.470,0.632)	(0,0)	(0,0)
mSP11	2204	933	-1144	35.6	+	(0,0)	(0.642,-0.400)	(0,0)
mSP11	1406	1471	-2078	8.3	+	(0,0)	(0,0)	(-0.130,-0.690)
mSP12	1371	1671	-6855	10.0	+	(0,0)	(0,0)	(0,0)
mSP12	1054	1372	-5754	13.7	-	(0,0)	(0,0)	(0,0)
mSP12	915	927	-3993	20.7	+	(0.078,0.833)	(0,0)	(0,0)
mSP12	826	1016	-3926	12.8	+	(0,0)	(-0.630,-0.490)	(0,0)
mSP12	1706	1287	-4436	29.7	+	(0,0)	(0,0)	(0.416,-0.260)
mSP13	524	800	-3315	15.0	+	(0,0)	(0,0)	(0,0)
mSP13	765	1192	-4924	12.0	-	(0,0)	(0,0)	(0,0)
mSP13	1055	1601	-6365	13.6	+	(0.277,-0.820)	(0,0)	(0,0)
mSP13	1073	1664	-6528	11.6	+	(0,0)	(0.728,0.060)	(0,0)
mSP13	540	774	-2432	5.3	+	(0,0)	(0,0)	(0.705,-0.201)
mSP20	1754	840	7385	13.3	-	(0,0)	(0,0)	(0,0)
mSP21	792	845	6404	12.6	-	(0,0)	(0,0)	(0,0)
NUSP10	718	467	1657	19.0	+	(0,0)	(0,0)	(0.023,-0.810)

Table 11: Benchmarks for the class SOP where the stop $\widetilde{t}_1$ is the NLSP in mSUGRA and in NUSUGRA models.

Higgs Patterns (HPs)

SUGRA Pattern	m_0 (GeV)	$m_{1/2}$ (GeV)	A_0 (GeV)	$\tan\beta$ (v_u/v_d)	μ (sign)	NUH $(\delta_{H_u}, \delta_{H_d})$	NU3 $(\delta_{q3}, \delta_{tbR})$	NUG $(\delta_{M_2}, \delta_{M_3})$
mSP14	1040	560	450	53.5	+	(0,0)	(0,0)	(0,0)
mSP14	760	515	2250	31.0	+	(0.255,-0.500)	(0,0)	(0,0)
mSP14	740	620	840	53.1	+	(0,0)	(-0.530,-0.249)	(0,0)
mSP14	1205	331	-710	55.0	+	(0,0)	(0,0)	(0.380,0.250)
mSP15	1110	760	1097	51.6	+	(0,0)	(0,0)	(0,0)
mSP15	1395	554	-175	59.2	+	(0,0)	(-0.040,0.918)	(0,0)
mSP15	905	500	1460	54.8	+	(0,0)	(0,0)	(-0.350,-0.260)
mSP16	520	455	620	55.5	+	(0,0)	(0,0)	(0,0)
mSP16	282	464	67	43.2	+	(0.912,-0.529)	(0,0)	(0,0)
NUSP12	2413	454	-2490	48.0	+	(0,0)	(0,0)	(-0.285,-0.848)

Table 12: Benchmarks for the class HP where the Higgs boson (A, H) is the next nearest heavy particle after the LSP in mSUGRA and in NUSUGRA. The LSP and (A, H) sometimes are seen to switch.

References

[1] D. Feldman, Z. Liu and P. Nath, *The landscape of sparticle mass hierarchies and their signature space at the LHC*, *Phys. Rev. Lett.* **99** (2007) 251802 [arXiv:0707.1873].

[2] D. Feldman, Z. Liu and P. Nath, *Light Higgses at the Tevatron and at the LHC and observable dark matter in SUGRA and D-branes*, *Phys. Lett.* **B 662** (2008) 190 [arXiv:0711.4591].

[3] A.H. Chamseddine, R. Arnowitt and P. Nath, *Locally supersymmetric grand unification*, *Phys. Rev. Lett.* **49** (1982) 970; *Nucleon decay in supergravity unified theories*, *Phys. Rev.* **D 32** (1985) 2348.

JHEP04(2008)054

[4] R. Barbieri, S. Ferrara and C.A. Savoy, *Gauge models with spontaneously broken local supersymmetry*, *Phys. Lett.* **B 119** (1982) 343.

[5] L.J. Hall, J.D. Lykken and S. Weinberg, *Supergravity as the messenger of supersymmetry breaking*, *Phys. Rev.* **D 27** (1983) 2359.

[6] For a review of supergravity models see, P. Nath, R. Arnowitt and A.H. Chamseddine, *Applied $N = 1$ supergravity*, Trieste Lectures (1983), World Scientific, Singapore (1984); H.P. Nilles, *Supersymmetry, supergravity and particle physics*, *Phys. Rept.* **110** (1984) 1; P. Nath, *Twenty years of SUGRA*, hep-ph/0307123.

[7] ATLAS collaboration, S. Yamamoto, *Strategy for early SUSY searches at ATLAS*, arXiv:0710.3953.

[8] V.S. Kaplunovsky and J. Louis, *Model independent analysis of soft terms in effective supergravity and in string theory*, *Phys. Lett.* **B 306** (1993) 269 [hep-th/9303040].

[9] A. Brignole, L.E. Ibáñez and C. Muñoz, *Towards a theory of soft terms for the supersymmetric standard model*, *Nucl. Phys.* **B 422** (1994) 125 [*Erratum ibid.* **436** (1995) 747] [hep-ph/9308271]; *Soft supersymmetry-breaking terms from supergravity and superstring models*, hep-ph/9707209.

[10] P. Nath and R. Arnowitt, *Non-universal soft SUSY breaking and dark matter*, *Phys. Rev.* **D 56** (1997) 2820 [hep-ph/9701301].

[11] A small sample of early works on the phenomenological implications of SUGRA models consists of S. Weinberg, *Upper bound on gauge fermion masses*, *Phys. Rev. Lett.* **50** (1983) 387;
R. Arnowitt, A.H. Chamseddine and P. Nath, *Masses of superpartners of quarks, leptons and gauge mesons in supergravity grand unified theories*, *Phys. Rev. Lett.* **50** (1983) 232; *Experimental signals for supersymmetric decays of the W and Z bosons*, *Phys. Lett.* **B 129** (1983) 445 [*Erratum ibid.* **132** (1983) 467]; *Gravity induced symmetry breaking and ground state of local supersymmetric guts*, *Phys. Lett.* **B 121** (1983) 33; *Model independent analysis of low-energy phenomena in supergravity unified theories*, HUTP-83/A077;
D.A. Dicus, S. Nandi, W.W. Repko and X. Tata, *Electron-positron annihilation cross-section in $\mathrm{SU}(2)_L \times \mathrm{U}(1)$ supergravity*, *Phys. Rev. Lett.* **51** (1983) 1030; *Electron spectra from wino decay at the $\bar{p}p$ collider*, *Phys. Rev.* **D 29** (1984) 67; *Lepton pair production as a signature of supersymmetry*, *Phys. Rev.* **D 29** (1984) 1317;
D.A. Dicus, S. Nandi and X. Tata, *W decay in supergravity guts*, *Phys. Lett.* **B 129** (1983) 451;
J.M. Frere and G.L. Kane, *On the possibility of finding light uncolored supersymmetric partners at present and future machines*, *Nucl. Phys.* **B 223** (1983) 331;
J.R. Ellis, J.M. Frere, J.S. Hagelin, G.L. Kane and S.T. Petcov, *Search for neutral gauge fermions in e^+e^- annihilation*, *Phys. Lett.* **B 132** (1983) 436;
J.R. Ellis, J.S. Hagelin, D.V. Nanopoulos and M. Srednicki, *Search for supersymmetry at the $\bar{p}p$ collider*, *Phys. Lett.* **B 127** (1983) 233;
M.K. Gaillard et al., *Light scalars in $N = 1$ locally supersymmetric theories*, *Phys. Lett.* **B 122** (1983) 355.

[12] S.P. Martin and P. Ramond, *Sparticle spectrum constraints*, *Phys. Rev.* **D 48** (1993) 5365 [hep-ph/9306314].

JHEP04(2008)054

[13] M. Drees and M.M. Nojiri, *The Neutralino relic density in minimal $N = 1$ supergravity*, *Phys. Rev.* **D 47** (1993) 376 [hep-ph/9207234];
P. Nath and R. Arnowitt, *Predictions in* SU(5) *supergravity grand unification with proton stability and relic density constraints*, *Phys. Rev. Lett.* **70** (1993) 3696 [hep-ph/9302318];
Cosmological constraints and SU(5) *supergravity grand unification*, *Phys. Lett.* **B 299** (1993) 58 [*Erratum ibid.* **307** (1993) 403] [hep-ph/9302317];
J.L. Lopez, D.V. Nanopoulos and K.-J. Yuan, *Accurate neutralino relic density computations in supergravity models*, *Phys. Rev.* **D 48** (1993) 2766 [hep-ph/9304216];
P. Nath and R. Arnowitt, *$B \to S\gamma$ decay in supergravity grand unification and dark matter*, *Phys. Lett.* **B 336** (1994) 395 [hep-ph/9406389];
G.L. Kane, C.F. Kolda, L. Roszkowski and J.D. Wells, *Study of constrained minimal supersymmetry*, *Phys. Rev.* **D 49** (1994) 6173 [hep-ph/9312272];
H. Baer and M. Brhlik, *Cosmological relic density from minimal supergravity with implications for collider physics*, *Phys. Rev.* **D 53** (1996) 597 [hep-ph/9508321];
J. Edsjo and P. Gondolo, *Neutralino relic density including coannihilations*, *Phys. Rev.* **D 56** (1997) 1879 [hep-ph/9704361];
U. Chattopadhyay, A. Corsetti and P. Nath, *Supersymmetric dark matter and Yukawa unification*, *Phys. Rev.* **D 66** (2002) 035003 [hep-ph/0201001];
H. Baer, C. Balázs and A. Belyaev, *Neutralino relic density in minimal supergravity with co-annihilations*, *JHEP* **03** (2002) 042 [hep-ph/0202076].

[14] U. Chattopadhyay, A. Corsetti and P. Nath, *WMAP constraints, SUSY dark matter and implications for the direct detection of SUSY*, *Phys. Rev.* **D 68** (2003) 035005 [hep-ph/0303201];
J.R. Ellis, K.A. Olive, Y. Santoso and V.C. Spanos, *Supersymmetric dark matter in light of WMAP*, *Phys. Lett.* **B 565** (2003) 176 [hep-ph/0303043];
H. Baer, A. Belyaev, T. Krupovnickas and J. O'Farrill, *Indirect, direct and collider detection of neutralino dark matter*, *JCAP* **08** (2004) 005 [hep-ph/0405210];
J. Edsjo, M. Schelke, P. Ullio and P. Gondolo, *Accurate relic densities with neutralino, chargino and sfermion coannihilations in mSUGRA*, *JCAP* **04** (2003) 001 [hep-ph/0301106];
P. Gondolo, J. Edsjo, P. Ullio, L. Bergstrom, M. Schelke and E.A. Baltz, *DarkSUSY: Computing supersymmetric dark matter properties numerically*, *JHEP* **07** (2004) 008 [astro-ph/0406204];
Y. Mambrini and E. Nezri, *Dark matter and colliders searches in the MSSM*, hep-ph/0507263;
M.M. Nojiri, G. Polesello and D.R. Tovey, *Constraining dark matter in the MSSM at the LHC*, *JHEP* **03** (2006) 063 [hep-ph/0512204];
J.L. Feng, A. Rajaraman and B.T. Smith, *Minimal supergravity with $m(0)^2 < 0$*, *Phys. Rev.* **D 74** (2006) 015013;
A. Belyaev, S. Dar, I. Gogoladze, A. Mustafayev and Q. Shafi, *Interplay of Higgs and sparticle masses in the CMSSM with updated SUSY constraints*, arXiv:0712.1049.

[15] R.R. de Austri, R. Trotta and L. Roszkowski, *A Markov chain Monte Carlo analysis of the CMSSM*, *JHEP* **05** (2006) 002 [hep-ph/0602028].

[16] B.C. Allanach, C.G. Lester and A.M. Weber, *The dark side of mSUGRA*, *JHEP* **12** (2006) 065;
B.C. Allanach, K. Cranmer, C.G. Lester and A.M. Weber, *Natural priors, CMSSM fits and LHC weather forecasts*, *JHEP* **08** (2007) 023.

JHEP04(2008)054

[17] P. Nath and R. Arnowitt, *Non-universal soft SUSY breaking and dark matter*, *Phys. Rev.* **D 56** (1997) 2820 [hep-ph/9701301];
A. Birkedal-Hansen and B.D. Nelson, *Relic neutralino densities and detection rates with nonuniversal gaugino masses*, *Phys. Rev.* **D 67** (2003) 095006 [hep-ph/0211071];
U. Chattopadhyay and D.P. Roy, *Higgsino dark matter in a SUGRA model with nonuniversal gaugino masses*, *Phys. Rev.* **D 68** (2003) 033010 [hep-ph/0304108];
D.G. Cerdeno and C. Munoz, *Neutralino dark matter in supergravity theories with non-universal scalar and gaugino masses*, *JHEP* **10** (2004) 015 [hep-ph/0405057];
G. Belanger, F. Boudjema, A. Cottrant, A. Pukhov and A. Semenov, *WMAP constraints on SUGRA models with non-universal gaugino masses and prospects for direct detection*, *Nucl. Phys.* **B 706** (2005) 411 [hep-ph/0407218];
H. Baer, A. Mustafayev, S. Profumo, A. Belyaev and X. Tata, *Direct, indirect and collider detection of neutralino dark matter in SUSY models with non-universal Higgs masses*, *JHEP* **07** (2005) 065 [hep-ph/0504001].

[18] B. Körs and P. Nath, *Hierarchically split supersymmetry with Fayet-Iliopoulos D-terms in string theory*, *Nucl. Phys.* **B 711** (2005) 112 [hep-th/0411201].

[19] D. Feldman, B. Körs and P. Nath, *Extra-weakly interacting dark matter*, *Phys. Rev.* **D 75** (2007) 023503 [hep-ph/0610133].

[20] V. Barger, C. Kao, P. Langacker and H.-S. Lee, *Neutralino relic density in a supersymmetric* U(1)′ *model*, *Phys. Lett.* **B 600** (2004) 104 [hep-ph/0408120].

[21] J.R. Ellis, S. Heinemeyer, K.A. Olive and G. Weiglein, *Indirect sensitivities to the scale of supersymmetry*, *JHEP* **02** (2005) 013 [hep-ph/0411216].

[22] L.S. Stark, P. Hafliger, A. Biland and F. Pauss, *New allowed mSUGRA parameter space from variations of the trilinear scalar coupling A*0, *JHEP* **08** (2005) 059 [hep-ph/0502197].

[23] A. Djouadi, M. Drees and J.-L. Kneur, *Updated constraints on the minimal supergravity model*, *JHEP* **03** (2006) 033 [hep-ph/0602001].

[24] J.R. Ellis, S. Heinemeyer, K.A. Olive and G. Weiglein, *Phenomenological indications of the scale of supersymmetry*, *JHEP* **05** (2006) 005 [hep-ph/0602220].

[25] U. Chattopadhyay, D. Das, A. Datta and S. Poddar, *Non-zero trilinear parameter in the mSUGRA model — Dark matter and collider signals at Tevatron and LHC*, *Phys. Rev.* **D 76** (2007) 055008 [arXiv:0705.0921].

[26] T. Bringmann, L. Bergstrom and J. Edsjo, *New gamma-ray contributions to supersymmetric dark matter annihilation*, *JHEP* **01** (2008) 049 [arXiv:0710.3169].

[27] A. Djouadi, J.-L. Kneur and G. Moultaka, *SuSpect: a Fortran code for the supersymmetric and Higgs particle spectrum in the MSSM*, *Comput. Phys. Commun.* **176** (2007) 426 [hep-ph/0211331].

[28] G. Bélanger, F. Boudjema, A. Pukhov and A. Semenov, *MicrOMEGAs*2.0*: a program to calculate the relic density of dark matter in a generic model*, *Comput. Phys. Commun.* **176** (2007) 367 [hep-ph/0607059]; *MicrOMEGAs: version 1.3*, *Comput. Phys. Commun.* **174** (2006) 577 [hep-ph/0405253]; *MicrOMEGAs: a program for calculating the relic density in the MSSM*, *Comput. Phys. Commun.* **149** (2002) 103 [hep-ph/0112278].

[29] F.E. Paige, S.D. Protopopescu, H. Baer and X. Tata, *ISAJET* 7.69*: a Monte Carlo event generator for p p, $\bar{p}p$ and e^+e^- reactions*, hep-ph/0312045.

JHEP04(2008)054

[30] W. Porod, *SPheno, a program for calculating supersymmetric spectra, SUSY particle decays and SUSY particle production at e^+e^- colliders*, *Comput. Phys. Commun.* **153** (2003) 275 [hep-ph/0301101].

[31] B.C. Allanach, *SOFTSUSY: a C++ program for calculating supersymmetric spectra*, *Comput. Phys. Commun.* **143** (2002) 305 [hep-ph/0104145].

[32] P. Nath, J.-Z. Wu and R. Arnowitt, *Landau pole effects and the parameter space of the minimal supergravity model*, *Phys. Rev.* **D 52** (1995) 4169 [hep-ph/9502388];
B. Allanach, S. Kraml and W. Porod, *Comparison of SUSY mass spectrum calculations*, hep-ph/0207314;
J.R. Ellis, K.A. Olive, Y. Santoso and V.C. Spanos, *Likelihood analysis of the CMSSM parameter space*, *Phys. Rev.* **D 69** (2004) 095004 [hep-ph/0310356];
M.E. Gomez, T. Ibrahim, P. Nath and S. Skadhauge, *Sensitivity of supersymmetric dark matter to the b quark mass*, *Phys. Rev.* **D 70** (2004) 035014 [hep-ph/0404025];
J.R. Ellis, S. Heinemeyer, K.A. Olive and G. Weiglein, *Indirect sensitivities to the scale of supersymmetry*, *JHEP* **02** (2005) 013 [hep-ph/0411216].

[33] H. Baer, J. Ferrandis, S. Kraml and W. Porod, *On the treatment of threshold effects in SUSY spectrum computations*, *Phys. Rev.* **D 73** (2006) 015010 [hep-ph/0511123].

[34] G. Bélanger, S. Kraml and A. Pukhov, *Comparison of SUSY spectrum calculations and impact on the relic density constraints from WMAP*, *Phys. Rev.* **D 72** (2005) 015003 [hep-ph/0502079].

[35] B.C. Allanach, A. Djouadi, J.L. Kneur, W. Porod and P. Slavich, *Precise determination of the neutral Higgs boson masses in the MSSM*, *JHEP* **09** (2004) 044 [hep-ph/0406166].

[36] B.C. Allanach, S. Kraml and W. Porod, *Theoretical uncertainties in sparticle mass predictions from computational tools*, *JHEP* **03** (2003) 016 [hep-ph/0302102]; *Comparison of SUSY mass spectrum calculations*, hep-ph/0207314.

[37] WMAP collaboration, D.N. Spergel et al., *Wilkinson Microwave Anisotropy Probe (WMAP) three year results: implications for cosmology*, *Astrophys. J. Suppl.* **170** (2007) 377 [astro-ph/0603449].

[38] G. Degrassi, P. Gambino and G.F. Giudice, *$B \to X/s\gamma$ in supersymmetry: large contributions beyond the leading order*, *JHEP* **12** (2000) 009 [hep-ph/0009337];
A.J. Buras, P.H. Chankowski, J. Rosiek and L. Slawianowska, *$\Delta(M(d,s)), B/(d,s)0 \to \mu^+\mu^-$ and $B \to X/s\gamma$ in supersymmetry at large* $\tan\beta$, *Nucl. Phys.* **B 659** (2003) 3 [hep-ph/0210145];
M.E. Gomez, T. Ibrahim, P. Nath and S. Skadhauge, *An improved analysis of $b \to s\gamma$ in supersymmetry*, *Phys. Rev.* **D 74** (2006) 015015 [hep-ph/0601163];
G. Degrassi, P. Gambino and P. Slavich, *QCD corrections to radiative B decays in the MSSM with minimal flavor violation*, *Phys. Lett.* **B 635** (2006) 335 [hep-ph/0601135] and the references therein.

[39] Heavy Flavor Averaging Group (HFAG) collaboration, E. Barberio et al., *Averages of B-hadron properties at the end of* 2006, arXiv:0704.3575.

[40] M. Misiak et al., *The first estimate of $B(\bar{B} \to X/s\gamma)$ at $O(\alpha_s^2)$*, *Phys. Rev. Lett.* **98** (2007) 022002 [hep-ph/0609232].

JHEP04(2008)054

[41] S.R. Choudhury and N. Gaur, *Dileptonic decay of B/s meson in SUSY models with large* $\tan\beta$, *Phys. Lett.* **B 451** (1999) 86 [hep-ph/9810307];
C. Bobeth, T. Ewerth, F. Krüger and J. Urban, *Analysis of neutral Higgs-boson contributions to the decays $\bar{B}/s \to \ell^+\ell^-$ and $\bar{B} \to K\ \ell^+\ell^-$*, *Phys. Rev.* **D 64** (2001) 074014 [hep-ph/0104284].

[42] CDF collaboration, A. Abulencia et al., *Search for $B_s \to \mu^+\mu^-$ and $B_d \to \mu^+\mu^-$ decays in $p\bar{p}$ collisions with CDF II*, *Phys. Rev. Lett.* **95** (2005) 221805 [*Erratum ibid.* **95** (2005) 249905] [hep-ex/0508036].

[43] D0 collaboration, V.M. Abazov et al., *Search for $B_s \to \mu^+\mu^-$ at D0*, *Phys. Rev.* **D 76** (2007) 092001 [arXiv:0707.3997].

[44] CDF collaboration and others, *Search for $B_s \to \mu^+\mu^-$ and $B_d \to \mu^+\mu^-$ Decays with $2fb-1$ of $p\bar{p}$ collisions*, arXiv:0712.1708.

[45] K. Anikeev et al., *B physics at the Tevatron: Run II and beyond*, hep-ph/0201071.

[46] LEP Working Group for Higgs boson searches collaboration, R. Barate et al., *Search for the standard model Higgs boson at LEP*, *Phys. Lett.* **B 565** (2003) 61 [hep-ex/0306033];
ALEPH, DELPHI, L3 and OPAL collaborations, *Search for neutral MSSM Higgs bosons at LEP*, LHWG-Note 2005-01.

[47] OPAL collaboration, G. Abbiendi et al., *Search for invisibly decaying Higgs bosons in $e^+e^- \to$ Zoho production at $\sqrt{s} = 183$-$209\ GeV$*, arXiv:0707.0373.

[48] OPAL collaboration, G. Abbiendi et al., *Search for chargino and neutralino production at $\sqrt{s} = 192\ GeV$ to 209-GeV at LEP*, *Eur. Phys. J.* **C 35** (2004) 1 [hep-ex/0401026].

[49] T.C. Yuan, R. Arnowitt, A.H. Chamseddine and P. Nath, *Supersymmetric electroweak effects on $g-2(\mu)$*, *Z. Physik* **C 26** (1984) 407;
D.A. Kosower, L.M. Krauss and N. Sakai, *Low-energy supergravity and the anomalous magnetic moment of the muon*, *Phys. Lett.* **B 133** (1983) 305;
J.L. Lopez, D.V. Nanopoulos and X. Wang, *Large $(g-2)\mu$ in* SU(5) $\times$ U(1) *supergravity models*, *Phys. Rev.* **D 49** (1994) 366 [hep-ph/9308336];
U. Chattopadhyay and P. Nath, *Probing supergravity grand unification in the Brookhaven $g-2$ experiment*, *Phys. Rev.* **D 53** (1996) 1648 [hep-ph/9507386];
T. Moroi, *The muon anomalous magnetic dipole moment in the minimal supersymmetric standard model*, *Phys. Rev.* **D 53** (1996) 6565 [*Erratum ibid.* **56** (1997) 4424] [hep-ph/9512396];
T. Ibrahim and P. Nath, *CP violation and the muon anomaly in $N = 1$ supergravity*, *Phys. Rev.* **D 61** (2000) 095008 [hep-ph/9907555].

[50] K. Hagiwara, A.D. Martin, D. Nomura and T. Teubner, *Improved predictions for $g-2$ of the muon and $\alpha_{\rm QED}(M_Z^2)$*, *Phys. Lett.* **B 649** (2007) 173 [hep-ph/0611102].

[51] R. Arnowitt et al., *Indirect measurements of the stau-neutralino* 1(0) *mass difference and mSUGRA in the co-annihilation region of mSUGRA models at the LHC*, *Phys. Lett.* **B 649** (2007) 73; *Determining the dark matter relic density in the mSUGRA stau-neutralino co-annhiliation region at the LHC*, arXiv:0802.2968.

[52] G.J. Gounaris, J. Layssac and F.M. Renard, *Remarkable virtual SUSY effects in $W^\pm$ production at high energy hadron colliders*, *Phys. Rev.* **D 77** (2008) 013003 [arXiv:0709.1789].

JHEP04(2008)054

[53] O. Buchmueller et al., *Prediction for the lightest Higgs boson mass in the CMSSM using indirect experimental constraints*, *Phys. Lett.* **B 657** (2007) 87 [arXiv:0707.3447].

[54] S.P. Martin, *Compressed supersymmetry and natural neutralino dark matter from top squark-mediated annihilation to top quarks*, *Phys. Rev.* **D 75** (2007) 115005 [hep-ph/0703097].

[55] A.V. Gladyshev, D.I. Kazakov and M.G. Paucar, *Light stops in the MSSM parameter space*, arXiv:0704.1429.

[56] B.C. Allanach et al., *The Snowmass points and slopes: benchmarks for SUSY searches*, in *Proc. of the APS/DPF/DPB summer study on the future of particle physics (Snowmass 2001)*, Snowmass, Colorado U.S.A. 30 Jun–21 Jul, N. Graf. ed., hep-ph/0202233.

[57] M. Battaglia et al., *Updated post-WMAP benchmarks for supersymmetry*, *Eur. Phys. J.* **C 33** (2004) 273 [hep-ph/0306219].

[58] CMS collaboration, G.L. Bayatian et al., *CMS technical design report, volume II: physics performance*, *J. Phys.* **G 34** (2007) 995.

[59] J. Lykken, *Missing energy with* 100 *inverse picobarns*, LHC New Physics Signatures Workshop, MCTP, Jan. (2008), online at http://www.umich.edu/~mctp/SciPrgPgs/events/2008/LHC2008/scipro1.html.

[60] M. Spiropulu, *SUSY@LHC.CERN.CH*, arXiv:0801.0318.

[61] G. Barenboim, P. Paradisi, O. Vives, E. Lunghi and W. Porod, *Light charged Higgs at the beginning of the LHC era*, arXiv:0712.3559.

[62] J.R. Ellis, S. Heinemeyer, K.A. Olive and G. Weiglein, *Light heavy MSSM Higgs bosons at large* $\tan\beta$, *Phys. Lett.* **B 653** (2007) 292 [arXiv:0706.0977].

[63] K.L. Chan, U. Chattopadhyay and P. Nath, *Naturalness, weak scale supersymmetry and the prospect for the observation of supersymmetry at the Tevatron and at the LHC*, *Phys. Rev.* **D 58** (1998) 096004 [hep-ph/9710473];
J.L. Feng, K.T. Matchev and T. Moroi, *Multi-TeV scalars are natural in minimal supergravity*, *Phys. Rev. Lett.* **84** (2000) 2322 [hep-ph/9908309];
H. Baer, C. Balázs, A. Belyaev, T. Krupovnickas and X. Tata, *Updated reach of the CERN LHC and constraints from relic density,* $b \to s\gamma$ *and* $a(\mu)$ *in the mSUGRA model*, *JHEP* **06** (2003) 054 [hep-ph/0304303].

[64] J.M. Frere, D.R.T. Jones and S. Raby, *Fermion masses and induction of the weak scale by supergravity*, *Nucl. Phys.* **B 222** (1983) 11.

[65] J.A. Casas, A. Lleyda and C. Muñoz, *Strong constraints on the parameter space of the MSSM from charge and color breaking minima*, *Nucl. Phys.* **B 471** (1996) 3 [hep-ph/9507294].

[66] A. Kusenko, P. Langacker and G. Segre, *Phase transitions and vacuum tunneling into charge and color breaking minima in the MSSM*, *Phys. Rev.* **D 54** (1996) 5824 [hep-ph/9602414].

[67] J.R. Ellis, T. Falk, K.A. Olive and M. Srednicki, *Calculations of neutralino stau coannihilation channels and the cosmologically relevant region of MSSM parameter space*, *Astropart. Phys.* **13** (2000) 181 [*Erratum ibid.* **15** (2001) 413] [hep-ph/9905481].

[68] M.E. Gomez, G. Lazarides and C. Pallis, *Yukawa unification,* $b \to s\gamma$ *and bino stau coannihilation*, *Phys. Lett.* **B 487** (2000) 313 [hep-ph/0004028].

JHEP04(2008)054

[69] A. Djouadi, M. Drees and J.-L. Kneur, *Neutralino dark matter in mSUGRA: reopening the light Higgs pole window*, *Phys. Lett.* **B 624** (2005) 60 [hep-ph/0504090].

[70] P. Skands et al., *SUSY Les Houches accord: interfacing SUSY spectrum calculators, decay packages and event generators*, *JHEP* **07** (2004) 036 [hep-ph/0311123].

[71] T. Sjostrand, S. Mrenna and P. Skands, *PYTHIA* 6.4 *physics and manual*, *JHEP* **05** (2006) 026 [hep-ph/0603175].

[72] See online http://www.physics.ucdavis.edu/~conway/research/software/pgs/pgs4-general.htm.

[73] W. Beenakker et al., *The production of charginos/neutralinos and sleptons at hadron colliders*, *Phys. Rev. Lett.* **83** (1999) 3780 [hep-ph/9906298].

[74] S. Jadach, Z. Was, R. Decker and J.H. Kuhn, *The tau decay library TAUOLA: version* 2.4, *Comput. Phys. Commun.* **76** (1993) 361.

[75] CMS COLLABORATION, *The CMS physics technical design report, volume* 1, CERN/LHCC 2006-001 (2006).

[76] M. Chiorboli, M. Galanti and A. Tricomi, *Leptons + jets + missing energy analysis at LM1*, CMS NOTE 2006/133.

[77] D.J. Mangeol and U. Goerlach, *Search for neutralino2 decays to tau-stau and SUSY mass spectrum measurement using di-tau final states*, CMS NOTE 2006/096.

[78] W. de Boer et al., *Trilepton final state from neutralino-chargino production in mSUGRA*, CMS NOTE 2006/113.

[79] N. Arkani-Hamed, G.L. Kane, J. Thaler and L.-T. Wang, *Supersymmetry and the LHC inverse problem*, *JHEP* **08** (2006) 070 [hep-ph/0512190].

[80] G.L. Kane, P. Kumar and J. Shao, *LHC string phenomenology*, *J. Phys.* **G 34** (2007) 1993.

[81] J.P. Conlon, C.H. Kom, K. Suruliz, B.C. Allanach and F. Quevedo, *Sparticle spectra and LHC signatures for large volume string compactifications*, *JHEP* **08** (2007) 061 [arXiv:0704.3403].

[82] H. Baer, V. Barger, G. Shaughnessy, H. Summy and L.-t. Wang, *Precision gluino mass at the LHC in SUSY models with decoupled scalars*, *Phys. Rev.* **D 75** (2007) 095010 [hep-ph/0703289].

[83] P.G. Mercadante, J.K. Mizukoshi and X. Tata, *Extending SUSY reach at the CERN Large Hadron Collider using b-tagging*, *Braz. J. Phys.* **37** (2007) 549.

[84] R. Kitano and Y. Nomura, *Supersymmetry, naturalness and signatures at the LHC*, *Phys. Rev.* **D 73** (2006) 095004 [hep-ph/0602096].

[85] H. Baer, K. Hagiwara and X. Tata, *Gauginos as a signal for supersymmetry at $p\bar{p}$ colliders*, *Phys. Rev.* **D 35** (1987) 1598.

[86] P. Nath and R. Arnowitt, *Supersymmetric signals at the Tevatron*, *Mod. Phys. Lett.* **A 2** (1987) 331;
R. Arnowitt, R.M. Barnett, P. Nath and F. Paige, *Weak gaugino production at the SSC*, *Int. J. Mod. Phys.* **A 2** (1987) 1113;
H. Baer, C.-H. Chen, F. Paige and X. Tata, *Trileptons from chargino-neutralino production at the CERN Large Hadron Collider*, *Phys. Rev.* **D 50** (1994) 4508 [hep-ph/9404212];

JHEP04(2008)054

V.D. Barger, C. Kao and T.-J. Li, *Trilepton signal of minimal supergravity at the Tevatron including tau-lepton contributions*, *Phys. Lett.* **B 433** (1998) 328 [hep-ph/9804451];
H. Baer, M. Drees, F. Paige, P. Quintana and X. Tata, *Trilepton signal for supersymmetry at the Fermilab Tevatron revisited*, *Phys. Rev.* **D 61** (2000) 095007 [hep-ph/9906233].

[87] G.J. Gounaris, J. Layssac and F.M. Renard, *Genuine SUSY signatures from $ug \to \tilde{d}\chi_i^+$ and $ug \to dW^+$, at high energies*, arXiv:0803.0813.

JHEP04(2008)054